Acid sphingomyelinase promotes mitochondrial dysfunction due to glutamate-induced regulated necrosis

Sergei A. Novgorodov,* Joshua R. Voltin,* Monika A. Gooz,[†] Li Li,[†] John J. Lemasters,[†] and Tatyana I. Gudz[1],*,[§]

Departments of Neuroscience* and Drug Discovery,[†] Medical University of South Carolina, Charleston, SC 29425; and Ralph H. Johnson Veterans Affairs Medical Center,[§] Charleston, SC 29401

Abstract Inhibiting the glutamate/cystine antiporter system x_c^-, a key antioxidant defense machinery in the CNS, could trigger a novel form of regulated necrotic cell death, ferroptosis. The underlying mechanisms of system x_c^--dependent cell demise were elucidated using primary oligodendrocytes (OLs) treated with glutamate to block system x_c^- function. Pharmacological analysis revealed ferroptosis as a major contributing factor to glutamate-initiated OL death. A sphingolipid profile showed elevations of ceramide species and sphingosine that were preventable by inhibiting of an acid sphingomyelinase (ASM) activity. OL survival was enhanced by both downregulating ASM expression and blocking ASM activity. Glutamate-induced ASM activation seems to involve posttranscriptional mechanisms and was associated with a decreased GSH level. Further investigation of the mechanisms of OL response to glutamate revealed enhanced reactive oxygen species production, augmented lipid peroxidation, and opening of the mitochondrial permeability transition pore that were attenuated by hindering ASM. Of note, knocking down sirtuin 3, a deacetylase governing the mitochondrial antioxidant system, reduced OL survival. **JLR** The data highlight the importance of the mitochondrial compartment in regulated necrotic cell death and accentuate the novel role of ASM in disturbing mitochondrial functions during OL response to glutamate toxicity, which is essential for pathobiology in stroke and traumatic brain injury.—Novgorodov, S. A., J. R. Voltin, M. A. Gooz, L. Li, J. J. Lemasters, and T. I. Gudz. **Acid sphingomyelinase promotes mitochondrial dysfunction due to glutamate-induced regulated necrosis.** *J. Lipid Res.* 2018. 59: 312–329.

Supplementary key words brain lipids • ferroptosis • glutamate/cystine antiporter • lipids/peroxidation • mitochondria • sphingolipids • sirtuin • oligodendrocytes

For many years, apoptosis was used as a synonym of programmed cell death, whereas the term necrosis was reserved for nonregulated cell death, which was not amenable to therapeutic manipulation. The recent discovery of regulated necrotic cell death mechanisms presents exciting possibilities for gaining control over cell survival in disease (1). The uncovering of necroptosis and ferroptosis as the alternative forms of programmed cell death has resulted in a few studies implicating regulated necrotic cell death as an important contributing factor in tumor suppression, neurodegeneration, and ischemia/reperfusion (IR) tissue injury (2, 3).

In the brain, cessation of blood flow followed by reoxygenation, IR, induces a complex cascade of events involving an energy failure and an alteration of ionic homeostasis that results in excessive release of neurotransmitters, in particular, glutamate, into the extracellular space (4). Microdialysis studies in both humans and rodents have also demonstrated a rise in extracellular glutamate following traumatic brain injury (TBI) (5). Glutamate can harm oligodendrocytes (OLs), unique myelin-forming cells in the CNS, and neurons by excitotoxicity, caused via sustained activation of ionotropic glutamate receptors and/or by blocking the cystine/glutamate antiporter, system x_c^-, leading to oxidative stress (6–8). System x_c^- is an amino acid antiporter that imports cystine, the oxidized form of cysteine, into cells with 1:1 countertransport of glutamate.

It is composed of a regulatory protein, SLC3A2 (4F2hc), linked by a disulfide bridge to the 12-pass transmembrane protein, SLC7A11 (xCT), which is credited for the transport activity of the dimer (9). The transport is driven by a transmembrane glutamate gradient and it can be inhibited by high extracellular glutamate, which is the only physiological inhibitor identified so far (10, 11).

Ferroptosis is believed to be distinct from other types of regulated cell death, such as apoptosis, necroptosis, and autophagic cell death at morphological, biochemical, and genetic levels (12, 13). Ferroptosis has been described as a form of regulated necrotic cell death characterized by excessive reactive oxygen species (ROS) generation and iron-dependent accumulation of lipid peroxidation products (13). Ferroptosis can be induced through inhibition of system x_c^- or by blocking glutathione peroxidase 4 function (3, 13). System x_c^- negatively regulates lipid peroxidation by providing cysteine, a substrate for biosynthesis of GSH that is required for activity of glutathione peroxidase 4, which reduces the accumulation of phospholipid peroxides and protects cells (1, 3). Blocking the system x_c^--dependent pathway has been considered as a promising cancer therapy (1). Yet, the mechanisms of system x_c^--mediated cell death in the neural cells and its relevance to neurological disease remain unclear. We hypothesized that high extracellular glutamate, a key factor in cerebral IR and TBI, could suppress the activity of the system x_c^-, leading to excessive ROS formation and OL death via ferroptosis.

Experimental evidence implicates sphingolipids, which are elevated in cerebral mitochondria after IR and TBI, as a causal factor of mitochondrial dysfunction and elevated ROS (14–18). We have previously reported the augmented sphingosine levels in brain tissue and mitochondria in an animal model of TBI (16). Several studies showed that sphingolipid ceramide increases in the brain after experimental stroke, and reduction of ceramide generation was neuroprotective, leading to smaller infarct sizes (19–21). Ceramides, a family of distinct molecular species characterized by various acyl chains, are synthesized de novo in the endoplasmic reticulum (ER) or generated through the recycling pathway from SM hydrolysis by acid sphingomyelinase (ASM) (15). ASM is a phosphodiesterase that converts SM, a structural component of membranes, into ceramide and phosphocholine (22). Hereditary mutations of ASM result in a toxic accumulation of SM in lysosomes and are the cause of Niemann-Pick disease. More recently, it was discovered that inhibition of ASM activity mediates the effects of antidepressant drugs (23) and diminishes symptoms associated with Alzheimer's disease (24).

In this study, we provide evidence for a critical role of ASM in mitochondrial dysfunction leading to system x_c^--dependent regulated necrotic OL death. Importantly, we show that ASM inhibitors or Smpd1 gene ablation preserves mitochondrial function, reduces ROS generation and oxidative lipid damage, and augments OL survival in response to glutamate. These studies suggest a novel mechanism of ASM involvement in regulated necrosis that could be an important contributing factor to brain injury in stroke and TBI.

MATERIALS AND METHODS

Animals and reagents

Female timed-pregnant Sprague-Dawley rats (Charles River Laboratories, Wilmington, MA) were acclimated for 1 week prior to experimentation. ASM-deficient mice were provided by the animal core facility at the Medical University of South Carolina (MUSC), Charleston SC (25). Experimental protocols were reviewed and approved by the Institutional Animal Care and Use Committee of MUSC and followed the National Institutes of Health guidelines for experimental animal use. DMEM/F12 and FBS used for cell culture were from GIBCO (Thermo Fisher, Waltham, MA). The complete protease inhibitor cocktail and PhosphoStop phosphatase inhibitor cocktail were from Roche Applied Science (Indianapolis, IN). Reclast (zoledronic acid), Z-VAD-fmk, and epoxyquinone G109 were from Enzo Biochem (Farmingdale, NY). Fumonisin B1 (FB1), myriocin, and GKT137831 were purchased from Cayman Chemical (Ann Arbor, MI). The 2′,7′-dichlorodihydrofluorescein (H2-DCF) diacetate, 4-acetamido-TEMPO, and MitoSox Red were from Thermo Fisher, C10-biphosphonate (C10-BPA) was from Avanti Polar Lipids (Alabaster, AL). Necrostatin-1 (methyl-thiohydantoin-tryptophan) and necrostatin-1s (7-Cl-O-necrostatin-1) were from BioVision (Milpitas, CA). LOXBlock-1 was from ChemBridge Corporation (San Diego, CA). GSK-872 and 4-amino-N-(3-chloro-4-fluorophenyl)-N′-hydroxy-1,2,5-oxadiazole-3-carboximidamide indolamine 2,3-deoxygenase (IDO) inhibitor were from EMD Millipore (Billerica, MA). NIM811 was generously provided by Novartis (Cambridge, MA). LCL-521 was provided by the Lipidomics Core facility at MUSC. All other chemicals were purchased from Sigma-Aldrich (St. Louis, MO).

Antibodies

Rabbit monoclonal anti-receptor-interacting protein kinase (RIPK)1, anti-RIPK3, anti-caspase-8, anti-LC3, anti-beclin-1 antibodies, and rabbit polyclonal anti-p62 antibodies were supplied by Cell Signaling Technology (Danvers, MA). Mouse monoclonal anti-β-actin antibody was from Sigma-Aldrich. Mouse monoclonal anti-RIPK1 antibody was purchased from R&D Systems (Minneapolis, MN). Rabbit polyclonal anti-ASM antibody was purchased from Santa Cruz Biotechnology (Santa Cruz, CA). Rabbit polyclonal anti-mixed-lineage kinase domain-like (MLKL) antibody was from Thermo Fisher. Secondary horseradish peroxidase-conjugated antibodies were supplied by Jackson ImmunoResearch (West Grove, PA).

Cell culture

Dissociated cortices of rat and mouse 2-day-old pups were cultured on poly-L-lysine (PLL)-coated flasks as described (26). Briefly, the cerebra of pups were dissected and minced to generate a single-cell suspension. Cells were plated into 75 cm^2 flasks and grown in DMEM/F12 medium with 10% FBS at 37°C and 5% CO$_2$. By day 10, mixed glial cultures were obtained, consisting of OLs and microglia growing on an astrocyte monolayer. OLs were purified from mixed glial cell cultures using a shake-off procedure. OLs were collected by centrifugation at 1,000 g for 5 min. OLs were used immediately for transfections or further culturing. Cell culture dishes and plates were precoated with PLL (50 µg/ml). Cells were plated in cell culture dishes and 96-well (4×10^5 cells/well) plates in DMEM/F12 medium with 10% FBS and N2 supplement and allowed 24 h for attachment. Cells were treated with glutamate and/or inhibitors in DMEM medium without cystine for a defined time. All cultures contained less than 2% of GFAP$^+$ astrocytes and nondetectable CD11$^+$ microglia.

RNAi

To downregulate ASM (Smpd1) and sirtuin 3 (SIRT3), ON-TARGET plus SMARTpool silencing RNAs were obtained from GE Healthcare/Dharmacon (Rockford, IL). The set consists of four siRNAs targeting different regions of the gene to minimize the off-target effects. The following target sequences were used: Smpd1, 5'-GAACAUAGCGCCACUAAAU-3', 5'-GCAACAGUCUC-GACAAGAU-3', 5'-GCAUAUAAUUGGGCACAUU-3', 5'-CGCCU-CAUCUCUCUCAAUA-3'; or Sirt3, 5'-GCUCAUGGGUCCUUU-GUAU-3', 5'-GGAUGGGACAGGACGGAUAA-3', 5'-CAGCAA-GGUUCUUACUACA-3', 5'-CAGCUUGUCUGAAUCGGUA-3'. OLs were transfected with siRNA using a Nucleofector electroporation system (Amaxa Biosystems, Gaithersburg, MD) according to the manufacturer's instructions with efficiencies of >70% as described (26). Cells (6×10^6) were mixed with 100 µl of Nucleofector reagent and 20 nM (1 µl) siRNA in the cuvette of the Amaxa electroporation device. ON-TARGET plus nontargeting pool siRNA (GE Healthcare/Dharmacon) was used as a control.

Cell survival assay

Cell death was measured using a lactate dehydrogenase (LDH)-based CytoTox-ONE™ homogeneous membrane integrity assay (Promega, Madison, WI) according to the manufacturer's recommendations. The fluorescence of the sample was measured at 590 nm emission with 560 nm excitation in a microplate reader (FLUOstar Optima; BMG LABTECH Inc., Durham, NC).

Caspase activity assay

The activities of executioner caspase 3/7 were determined using an Apo-One® homogeneous kit (Promega) according to the manufacturer's instructions. Cleavage of nonfluorescent substrate, Z-DEVD-Rodamine-110, by caspase 3/7 resulted in fluorescent Rodamine-110. The fluorescence of the sample was measured at 530 nm emission and 490 nm excitation in the microplate reader, Synergy H1 (BioTek, Winooski, VT).

Isolation of mitochondria

Mitochondria were isolated from OLs using a hypotonic swelling procedure (27).

Cell respiration

OLs (3×10^5 cells/well) were plated on 96-well Seahorse XF-96 plates (Seahorse Biosciences, Billerica, MA) coated with PLL and maintained in DMEM/F12 medium for 24 h in humidified 5% CO_2/95% air at 37°C. OLs were treated with glutamate in cystine-free medium for 6 h, then the medium was replaced with DPBS (PBS containing Ca^{2+} and Mg^{2+}) supplemented with 10 mM glucose, respiration [oxygen consumption rate (OCR)] was measured in a Seahorse Bioscience XF-96 extracellular flux analyzer, and respiratory rates were calculated using Seahorse XF-96 software and the Direct ACOS fast algorithm with continuous averaging, as described (28).

Confocal microscopy

Cells in modified HBSS were loaded (30 min at 37°C) with 200 nM TMRM or 5 µM MitoSox Red. After loading and washing, subsequent incubations were performed with 50 nM TMRM or 1 µM MitoSox Red to maintain equilibrium distribution of the fluorophore (29). Cells incubated in HBSS in humidified 5% CO_2/air at 37°C were imaged with a Zeiss LSM 510 NLO inverted laser scanning confocal/multiphoton microscope (Thornwood, NJ) using a 63×1.4 N.A. plan apochromat oil immersion lens. Fluorescence of TMRM was detected at 560 nm (excitation 543 nm) or fluorescence of MitoSox Red was detected at 580 nm (excitation 510 nm) through a filter and a 1 airy unit-diameter pinhole.

ROS generation

After the treatment with glutamate and test compounds, cells were washed three times with DPBS and incubated in the presence of 2 µM H2-DCF diacetate in DPBS supplemented with 10 mM glucose (DPBS buffer) at 37°C. Cellular ROS formation was assessed by oxidation of H2-DCF. Fluorescence of oxidized H2-DCF was measured at 520 nm emission and 490 nm excitation in the microplate reader, Synergy H1 (BioTek). Mitochondrial ROS formation was measured using MitoSox Red fluorescent dye. Cells were incubated with 5 µM MitoSox Red (Molecular Probes) in DPBS buffer for 30 min at 37°C to allow the dye to reach mitochondria. Cells were washed twice with DPBS buffer to remove excess dye. Fluorescence was measured at 580 nm emission and 510 nm excitation in the Synergy H1 microplate reader.

ASM and neutral sphingomyelinase activity assay

ASM activity was measured using an ASM activity assay kit (Echelon Biosciences, Salt Lake City, UT) according to the manufacturer's instructions. Neutral sphingomyelinase (NSM) activity was determined as described for the ASM assay, except that the reaction mixture contained 100 mM Tris (pH 7.4) instead of 100 mM sodium acetate (pH 5.0) and was supplemented with 10 mM Mg^{2+}, which is required for NSM activity (26).

GSH content

GSH content was determined using a glutathione fluorometric assay kit (BioVision) according to the manufacturer's instructions.

Lipid peroxidation measurements

After the treatment with glutamate and test compounds for 18 h, cells were incubated in the presence of 1 µM of BODIPY 581/591 C11, a fluorescent reporter for lipid peroxidation, for 1 h. Upon oxidation, the reagent shifts the fluorescence excitation/emission peak from 581/591 nm to 488/510 nm. The ratio of fluorescence intensities at 590 nm to 510 nm gives the read-out for lipid peroxidation. Lipid peroxidation products were measured using a malondialdehyde (MDA) assay kit (Sigma-Aldrich) according to the manufacturer's instructions.

Immunoprecipitation

Immunoprecipitations were performed as we previously described (17, 30, 31). For immunoprecipitation, cell lysates (500 µg) were precleared in buffer A [0.15 M NaCl, 0.5 mM EDTA, 0.5% Igepal CA-630, protease and phosphatase inhibitor cocktail, 0.05 M Tris (pH 7.5), and 0.2% BSA] by incubation with appropriate species-specific IgG-conjugated magnetic beads (Dynabeads, Dynal; Thermo Fisher) for 1 h. Antibodies were then added. After incubation at 4°C overnight with gentle mixing, antibody-antigen complexes were captured with Dynabeads and washed two times with buffer A (without BSA), and then washed twice with TBS (pH 7.5). The immunoprecipitates were eluted by boiling in SDS-sample buffer. As a control, the same immunoprecipitation procedure was performed except for the primary antibody application.

Western blot

Proteins were analyzed by Western blot (17, 30). Proteins were separated by 4–15% SDS-PAGE, blotted to PVDF membrane, blocked with 5% nonfat dry milk (Bio-Rad, Hercules, CA) or 5% BSA in TBS-T buffer [10 mM Tris, 150 mM NaCl, and 0.2% Tween-20 (pH 8.0)] and subsequently probed with the appropriate primary antibody. Immunoreactive bands were visualized using a SuperSignal West Dura substrate (Thermo Fisher).

Sphingolipid analysis

Sphingolipid content was determined by MS/MS (14, 17). Briefly, to extract lipids, 0.5 mg of mitochondria or cell lysate protein was added to 2 ml of the ethyl acetate/isopropanol/water (60:30:10%, v/v/v) solvent system. The lipid extracts were fortified with internal standards, dried under a stream of nitrogen gas, and reconstituted in 100 µl of methanol for ESI-MS/MS analysis, which was performed on a Thermo Fisher TSQ Quantum triple quadrupole mass spectrometer, operating in a multiple reaction-monitoring positive-ionization mode. The samples were injected onto the HP1100/TSQ Quantum liquid chromatography/MS system and gradient-eluted from the BDS Hypersil C8, 150 × 3.2 mm, 3 µm particle size column, with a 1.0 mM methanolic ammonium formate 2 mM aqueous ammonium formate mobile-phase system. The peaks for the target analytes and internal standards were collected and processed with the Xcalibur software system. Calibration curves were constructed by plotting peak area ratios of synthetic standards, representing each target analyte, to the corresponding internal standard. The target analyte peak area ratios from the samples were similarly normalized to their respective internal standard and compared with the calibration curves using a linear regression model. Each sample was normalized to its respective total protein levels.

Statistical analysis

Data were analyzed for statistically significant differences between groups by one-way ANOVA or Student's t-test where appropriate (SigmaPlot software version 12.0). Statistical significance was ascribed to the data when $P < 0.05$.

RESULTS

Glutamate-induced OL demise does not engage necroptotic or autophagic signaling mechanisms

OLs were treated with various concentrations of glutamate in cystine-free medium for 24 h. Relative cell survival was determined using a LDH-based assay, which measures a release of cytosolic LDH from the cells providing the quantification of the plasma membrane integrity. Consistent with previous reports (7, 32), glutamate-triggered OL death was attenuated by cystine, supporting the involvement of the glutamate/cystine antiporter, system x_c^- (**Fig. 1A**). To rule out the contribution of ionotropic glutamate receptor-mediated Ca^{2+}-dependent mechanisms, OLs were pretreated with 10 µM of the intracellular Ca^{2+} chelator, BAPTA-AM, for 1 h and then exposed to glutamate. OL survival was determined 24 h later. There was no effect of BAPTA on glutamate-induced OL death (not shown), indicating a lack of involvement of excitotoxicity mechanisms mediated by ionotropic glutamate receptors. The pan-caspase inhibitor, Z-VAD-fmk, failed to protect OLs from glutamate toxicity (Fig. 1B). Moreover, there was no executioner caspase 3/7 activation in response to glutamate, indicating that OL loss was not mediated by a caspase-dependent apoptotic mechanism (Fig. 1C). We have previously reported that OL exposure to glutamate in cystine-containing medium resulted in an activation of caspase 3/7
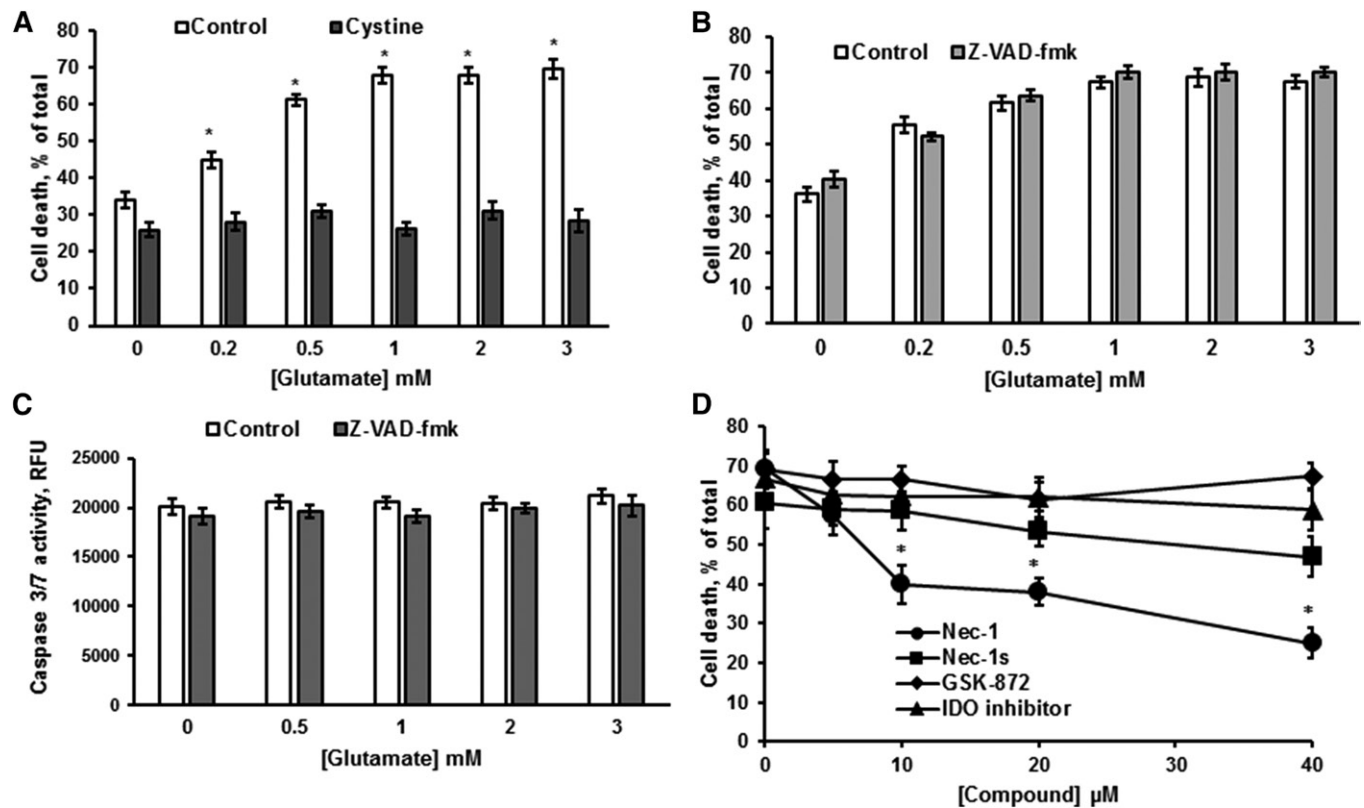
Fig. 1. Glutamate-elicited OL death does not involve apoptotic signaling mechanisms. OLs were treated with glutamate alone and in the presence of 1 mM cystine (A) or 30 µM ZVAD-fmk (B) for 24 h and cell survival was determined. Data are mean ± SE, *$P < 0.05$, n = 9. C: OLs were treated with glutamate with/without 30 µM Z-VAD-fmk for 24 h and caspase 3/7 activity was measured. Data are mean ± SE, n = 6. D: Cells were exposed to 1 mM glutamate in the presence of the necroptosis inhibitors, necrostatin-1 (Nec-1) and necrostatin-1s (Nec-1s), GSK-872, a RIP3 kinase inhibitor, and an IDO inhibitor. Cell survival was determined 24 h later. Data are mean ± SE, *$P < 0.05$, n = 9.

and Ca^{2+}-dependent apoptotic mechanism of OL demise (31). Lack of caspase 3/7 activation and Ca^{2+} involvement in OL death following treatment with glutamate in cystine-free medium (Fig. 1C) indicates that cystine is an important factor controlling the mechanisms of OL survival.

Various stimuli can engage a nonapoptotic form of cell death called necroptosis that is a regulated programmed necrosis (2). Necroptosis, like unprogrammed necrosis, is characterized by cellular organelles swelling and the rupture of the plasma membrane. Central molecular components of necroptosis signaling include RIPK1 and RIPK3 (33). The initiation of necroptosis leads to activation of RIPK1 and RIPK3 and formation of a multi-protein complex necrosome, which includes a key downstream target of RIPK3, a MLKL pseudokinase. MLKL does not regulate necrosome assembly, but is required for RIPK3 to kill cells following its binding and phosphorylation by RIPK3 (34). To determine whether OL treatment with glutamate initiates the necroptotic cell death cascade, we employed necrostatin-1, a cell-permeable inhibitor of RIPK1 activity (EC_{50} = 490 nM) and its more potent analog, necrostatin-1s (EC_{50} = 210 nM) (35). Figure 1D shows that necrostatin-1 significantly augmented OL survival, whereas necrostatin-1s was not effective. It has also been reported that necrostatin-1 could inhibit the activity of IDO, whereas necrostatin-1s lacks the activity against IDO (35). To distinguish between necrostatin-1 targeting necroptosis and IDO-related processes, we used a cell-permeable competitive IDO inhibitor, which lacks the activity toward necroptosis. The IDO inhibitor did not have any effect on OL survival in response to glutamate (Fig. 1D). The data suggest that OL protection by necrostatin-1 seems to implicate

other proteins than its canonical target, RIPK1. Furthermore, a selective inhibitor of RIPK3 activity, GSK-872 (36), did not impact OL survival, ruling out the engagement of RIPK3-mediated pathways.

Among several control mechanisms governing core necroptosis mediators, caspase-8 certainly plays an important role. Caspase-8 could initiate apoptosis and prevent necroptosis through cleavage of multiple pronecroptotic proteins, including RIPK1 and RIPK3. Depending on the availability of downstream molecules, cells die via necroptosis (if caspase-8 is lacking or inhibited) or apoptosis (if MLKL is absent) (33). To validate the presence of key necroptosis mediators in OLs, the expression of RIPK1, RIPK3, MLKL, and caspase-8 was determined in untreated cells and OLs treated with glutamate with/without necrostatin-1. Although RIPK1, RIPK3, MLKL, and caspase-8 were expressed in OLs, there were no changes in the expression of necroptosis mediators in response to glutamate treatment (**Fig. 2A**). Of note, immunoprecipitation studies using RIPK1 and RIPK3 antibodies showed no formation of necrosome complex in OLs following glutamate exposure (Fig. 2B). The data suggest that glutamate-induced OL death does not engage necroptosis machinery.

Emerging evidence indicates that the execution of cell death requires an orchestrated interplay between three important processes: apoptosis, necrosis, and autophagy. It has been reported that activating autophagy could protect from nutrient- and energy-deprivation-induced necroptosis (37). To assess a possible involvement of the autophagic pathway, key autophagy markers, including LC3A, beclin-1, and p62, were examined in OLs treated with glutamate (Fig. 2C). There was no impact of glutamate on the key
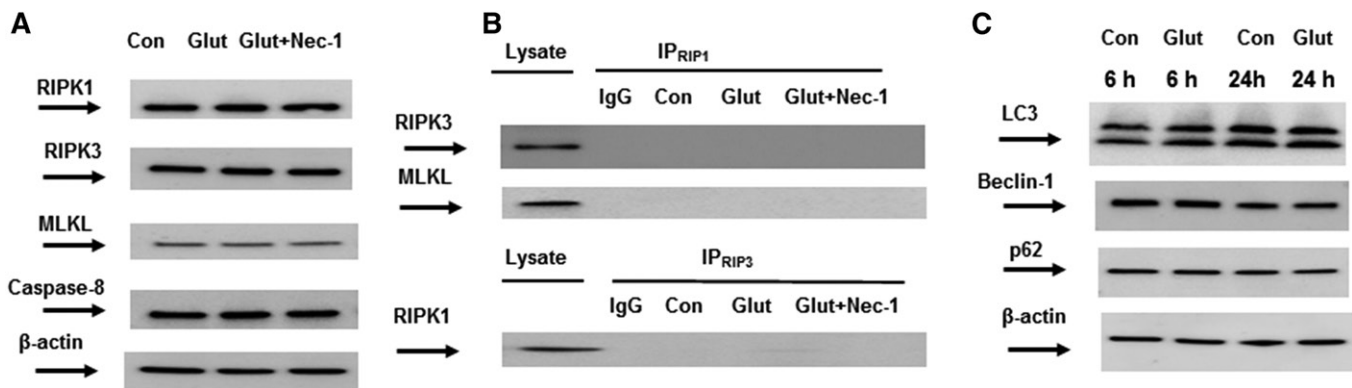
Fig. 2. OL demise in response to glutamate is not mediated by necroptotic or autophagic signaling machinery. A: OLs were exposed to 1 mM glutamate (Glut) with/without 40 µM necrostatin-1 (Nec-1) for 24 h and cell lysates were analyzed by Western blotting using anti-RIPK1 (Cell Signaling Technology), anti-RIPK3 (Cell Signaling Technology), anti-MLKL (Thermo Fisher), and anti-caspase-8 (Cell Signaling Technology) antibodies. To confirm equal loading of samples, the membranes were stripped and probed with anti-β-actin (Sigma-Aldrich) antibody. Data are representative of three independent experiments. Con, control. B: Necrosome complex formation was probed in immunoprecipitation experiments. OLs were treated with 1 mM glutamate (Glut) with/without 40 µM necrostatin-1 (Nec-1) for 24 h. Cell lysates were immunoprecipitated with anti-RIPK1 antibodies (R&D Systems) and probed using anti-RIPK3 (Cell Signaling Technology) or anti-MLKL (Thermo Fisher) antibodies. In reciprocal experiments, cell lysates were immunoprecipitated with anti-RIPK3 antibodies (Cell Signaling Technology) and probed using anti-RIPK1 antibodies (R&D Systems). Input load: 20 µg/lane. As a control, the same immunoprecipitation procedure was performed except for primary antibody application (IgG). C: OLs were exposed to 1 mM glutamate (Glut) for 6 h or 24 h and the cell lysates' (20 µg/lane) expression of autophagy markers was assessed by Western blotting using anti-LC3A (Cell Signaling Technology), anti-beclin-1 (Cell Signaling Technology), and anti-p62(Cell Signaling Technology) antibodies. To confirm equal loading of samples, the membranes were stripped and probed with anti-β-actin (Sigma-Aldrich) antibody. Data are representative of three independent experiments.

autophagy mediators' expression in OLs, ruling out the contribution of autophagic mechanisms.

Pharmacologic inhibitors of ferroptosis protect OLs from glutamate toxicity

Ferroptosis, a form of regulated necrosis, is characterized by excessive ROS generation and iron-dependent accumulation of lipid peroxides (38). Most inhibitors of ferroptosis are anti-oxidants or iron chelators. High-throughput screening efforts have identified ferrostatin-1 and liproxstatin-1 as highly potent and specific inhibitors of ferroptosis, which was ascribed to their ability to slow the accumulation of lipid peroxides (39) and by acting as radical-trapping antioxidants (40). Importantly, ferrostatin-1 and liproxstatin-1 have been shown to protect against IR tissue injury in vivo (12). Another group of compounds with a specific anti-ferroptotic activity is lipoxygenase inhibitors. Lipoxygenases oxygenate free or esterified fatty acids at various positions, thereby generating hydroperoxyl intermediates that promote lipid peroxidation. Zileuton, a 5-lipoxygenase inhibitor, and LOXBlock-1, a 12/15-lipoxygenase inhibitor, have been shown to protect cells in several in vitro models of ferroptosis (12). Furthermore, the NADPH oxidase (NOX) family of superoxide-producing enzymes (NOX1–5) has been implicated in promoting ferroptosis in cancer cell lines (38). Thus, inhibition of NOX1/4 with GKT137831 protected HT-1080 cells from ferroptosis induced by inhibiting system x_c^- with erastin (13). Of note, the NOX2 inhibitor, apocynin, improved neuronal survival and attenuated the infarct size in an animal stroke model (41).

To determine whether glutamate-initiated OL death involves the mechanisms and signaling pathways of ferroptosis, several specific inhibitors of ferroptosis were utilized. There was a significant OL protection against glutamate toxicity by ferrostatin-1 (Fig. 3A), liproxstatin-1 (Fig. 3B), zileuton (Fig. 3A), and LOXBlock-1 (**Fig. 3A**). Importantly, ferroptosis inhibitors significantly reduced OL death in both control cells and cells treated with glutamate in a concentration-dependent manner (not shown). The data indicate that OLs underwent ferroptotic cell death at the baseline in cystine-free medium. Furthermore, iron chelators, CPX (Fig. 3A) and deferoxamine (DFA) (Fig. 3C), augmented OL survival. Antioxidants, such as hydrophilic N-acetylcysteine (NAC) (Fig. 3C) and lipophilic vitamin E homologs 2,2,5,7,8-pentamethyl-6-chromanol (PMC) (Fig. 3B) and trolox (Fig. 3D), significantly reduced OL demise. The NOX inhibitors, apocynin (Fig. 3C) and GKT137831 (Fig. 3D), increased OL survival. The data suggest that OL exposure to glutamate triggers ferroptotic cell death.

To elucidate the intracellular compartments engaged by ferroptotic oxidative mechanisms, a mitochondria-targeted
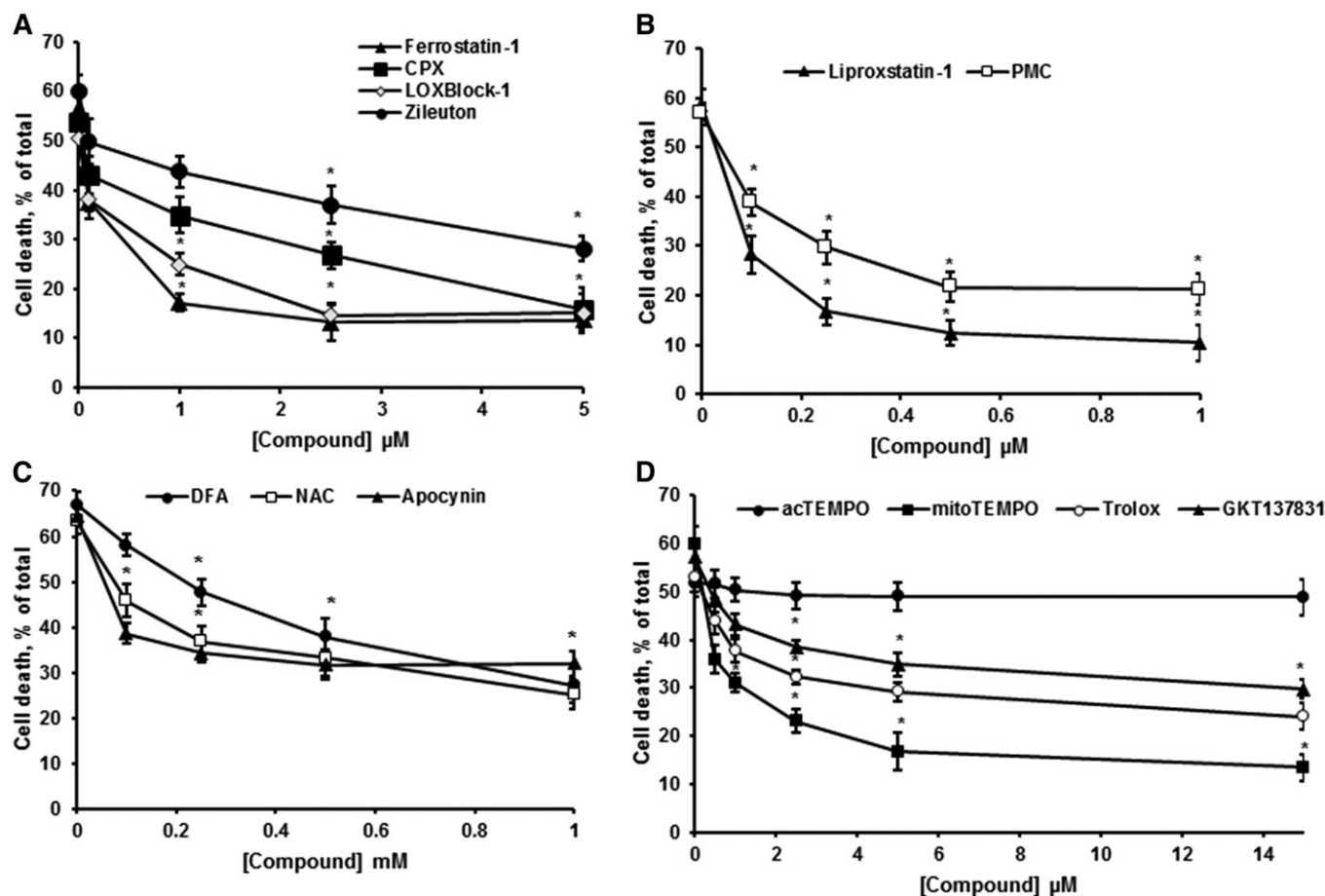

Fig. 3. OL survival in response to glutamate was augmented by ferroptosis inhibitors. A–D: OLs were treated with 1 mM glutamate in the presence of inhibitors for 24 h and relative cell survival was determined. Data are mean ± SE, *$P < 0.05$, n = 12.

antioxidant, mitoTEMPO, and its analog, 4-acetamido-2,2,6,6-tetramethylpiperidine 1-oxyl (acTEMPO), which is devoid of mitochondria-targeting moieties, were employed. mitoTEMPO is a mitochondria-targeted superoxide dismutase mimetic that possesses superoxide and alkyl radical scavenging properties. This compound combines the antioxidant piperidine nitroxide, TEMPO, with the lipophilic cation, triphenylphosphonium, which allows it to pass through lipid bilayers and accumulate in mitochondria (42). Figure 3D shows that mitoTEMPO augmented OL survival in response to glutamate, whereas acTEMPO did not have any effect. The data point to the importance of intra-mitochondrial oxidative mechanisms in glutamate-induced ferroptosis in OLs.

Glutamate treatment results in activation of SM hydrolysis in OLs

A hallmark of OL metabolism is the generation of large quantities of sphingolipids, which are key lipid components of myelin. Sphingolipids, ubiquitous structural components of cellular membranes, have emerged as a new class of lipid biomodulators of cell proliferation, differentiation, migration, autophagy, and apoptosis (15, 43). The bioactive sphingolipid metabolites, ceramide and sphingosine, have been shown to promote apoptotic cell death, while sphingosine-1 phosphate has been implicated in mediating cell proliferation and survival. Most sphingolipids of mammalian cellular membranes contain long fatty acyl chains of 14–28 carbon atoms, rendering them extremely

hydrophobic lipids. As a result, sphingolipid metabolism is restricted to cellular membranes and is highly compartmentalized (44). De novo synthesis of bioactive sphingolipids occurs in the ER and commences with generation of ceramide, which is then transported to the Golgi and plasma membrane for biosynthesis of SM (44). Another major source of bioactive sphingolipids is the degradation of SM by ASM yielding ceramide, which takes place in lysosomes (45). Ceramide is further hydrolyzed by acid ceramidase to form sphingosine, which could leave the lysosome and reach other intracellular compartments, such as the ER and mitochondria. In contrast, transfer of ceramide between intracellular compartments requires either the vesicular transport pathway or involves a transfer protein, CERT (45). In addition, SM could be hydrolyzed by Mg^{2+}-dependent NSM localized at the inner leaflet of the plasma membrane (46).

To explore the role of bioactive sphingolipids in OL response to glutamate, the sphingolipid profile was determined using a MS/MS lipidomics approach (**Fig. 4**). OL treatment with glutamate significantly increased ceramide and sphingosine content, while SM was reduced (Fig. 4A). The sphingolipid changes were prevented by cystine, confirming that glutamate's effect is mediated by blocking system x_c^- function. The content of intermediates of the de novo sphingolipid synthesis, dihydroceramide and dihydrosphingosine, was not affected, suggesting a lack of sphingolipid biosynthesis activation (Fig. 4A). Consistent with the reduced SM, ceramide and sphingosine increases
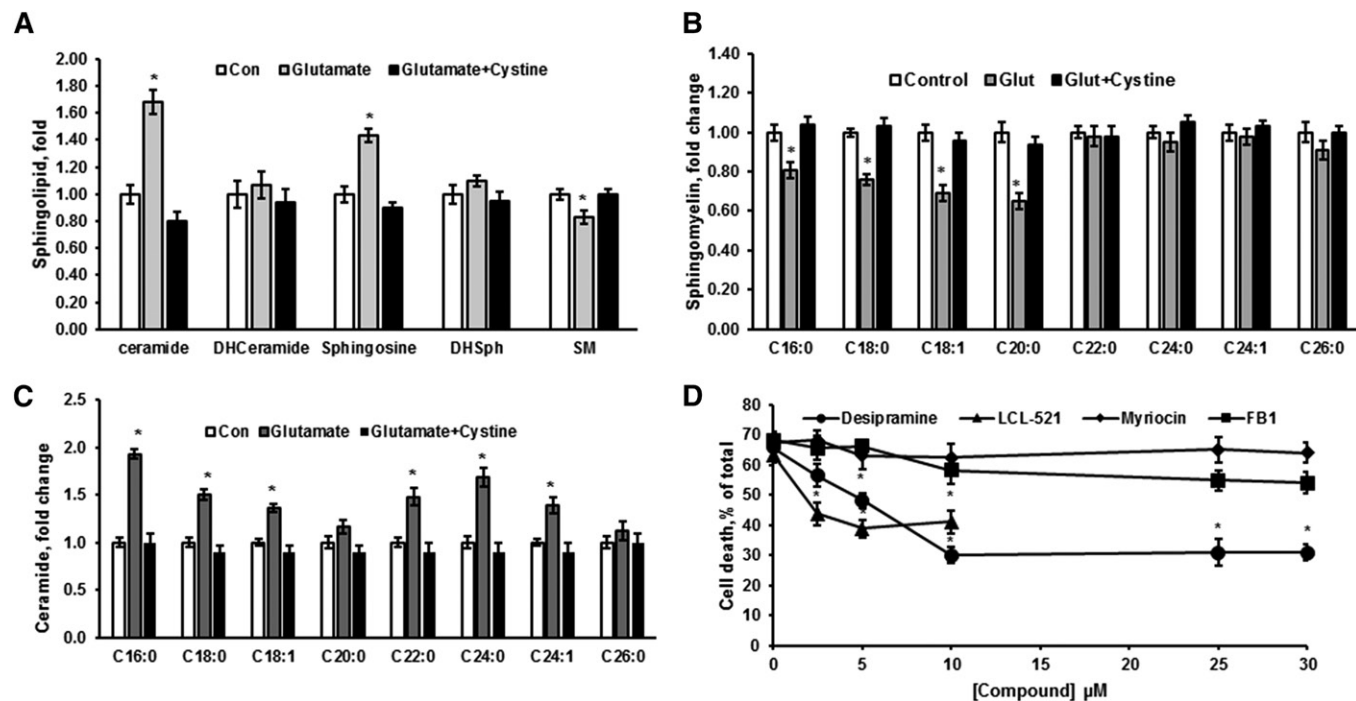
Fig. 4. Sphingolipid changes in glutamate-treated OLs indicate activation of SM hydrolysis. Sphingolipids were analyzed in OLs treated with 1 mM glutamate alone and in the presence of 1 mM cystine for 24 h. Total ceramide, sphingosine, SM, dihydroceramide (DHCeramide), and dihydrosphingosine (DHSph) (A), SM species (B), and ceramide species (C) were quantified. Data are mean ± SE, *P< 0.05, n = 8. Each sample was normalized to its respective total protein levels. D: OLs were exposed to 1 mM glutamate with/without inhibitors of de novo sphingolipid synthesis, including myriocin and FB1 or SM hydrolysis pathway (desipramine and LCL-521) for 24 h and relative cell survival was determined. Data are mean ± SE, *P< 0.05, n = 12.

seem to be due to activation of SM hydrolysis elicited by OL treatment with glutamate.

The content of SM species characterized by long-chain fatty acid, including $C_{16:0}$-, $C_{18:0}$-, $C_{18:1}$-, and $C_{20:0}$-SM, was decreased, whereas the content of SM species containing very long-chain fatty acid, $C_{22:0}$-, $C_{24:0}$-, $C_{24:1}$-, and $C_{26:0}$-SM, did not change (Fig. 4B). Ceramide species containing long-chain fatty acid, such as $C_{16:0}$-, $C_{18:0}$-, and $C_{18:1}$-ceramide, were increased, while $C_{20:0}$-ceramide was unchanged (Fig. 4C). The content of ceramide species containing very long-chain fatty acid, including $C_{22:0}$-, $C_{24:0}$-, and $C_{24:1}$-ceramide, was elevated, whereas $C_{26:0}$-ceramide did not change. The increase in ceramide species containing long-chain fatty acid was associated with reduced SM species, indicating that these ceramide species are generated from SM hydrolysis, potentially by ASM.

Importantly, a lack of the hydrolysis of SM species containing very long-chain fatty acids suggests that the increased ceramide species containing very long-chain fatty acids are not produced via ASM-mediated hydrolysis of SM in lysosomes. These ceramide species could be generated from sphingosine by ceramide synthase (CerS) in another intracellular compartment, such as mitochondria and/or ER, where CerS isoforms are expressed. Each of six known CerS proteins displays a distinct substrate specificity profile for fatty acid acyl-CoA: CerS1 generates $C_{18:0}$- and $C_{18:1}$-ceramide; CerS2 and CerS4 produce $C_{20:0}$-, $C_{24:0}$-, and $C_{24:1}$-ceramide; and CerS5 and CerS6 generate $C_{14:0}$-, $C_{16:0}$-, $C_{18:0}$-, and $C_{18:1}$-ceramide. In brain, the ER contains CerS1, -2, -4, -5, and -6, whereas mitochondria express CerS1, -2, -4, and -6 (14, 17). The data suggest that the products of SM hydrolysis, ceramides containing very long-chain fatty acid, are likely generated by CerS2 or CerS4 from sphingosine in the mitochondria and/or ER.

To investigate the role of sphingolipids and sphingolipid-metabolizing enzymes in glutamate-induced OL response, the impact of pharmacological inhibitors of sphingolipid-metabolizing enzyme activity on OL survival was determined (Fig. 4D). In line with the sphingolipid profile changes (Fig. 4A), a specific inhibitor of the de novo ceramide synthesis, myriocin, did not have any effect on OL survival. Desipramine, a selective inhibitor of lysosomal ASM, and LCL-521, a specific inhibitor of lysosomal acid ceramidase (47), significantly augmented OL survival. Desipramine, a clinically used antidepressant, is an indirect ASM inhibitor (48). ASM appears to be bound to intralysosomal membranes, thereby being protected against proteolytic inactivation. Protonated bases (desipramine and related drugs) accumulate in the acidic lysosomal compartment and hinder ASM binding to the inner membrane, resulting in selective proteolytic degradation of the enzyme without disturbing the integrity of the lysosome (49). The protective effect of desipramine on OL survival suggests an evident role for ASM in glutamate-induced OL death. Of note, FB1, a specific inhibitor of CerS, did not significantly improve OL survival. The data suggest that OL exposure to glutamate resulted in activation of SM hydrolysis by ASM, generating ceramide that was, in part, further metabolized into sphingosine by acid ceramidase in lysosomes. Sphingosine appears to be converted into ceramide by CerS, which is not localized in lysosomes, but rather in mitochondria and/or the ER. The lack of the CerS inhibitor's impact on cell survival suggests that ceramide is dispensable for glutamate-triggered regulated necrotic OL death.

ASM activation is required for glutamate-induced ferroptosis in OLs

The breakdown of SM to ceramide and phosphorylcholine is catalyzed by sphingomyelinase family enzymes, which can be distinguished on the basis of the optimal pH values required for their activation: acid (ASM) and neutral (NSM) (46). ASM is encoded by the SMPD1 gene and translates into a 629 amino acid pro-protein, which, because of differential modification and trafficking processes, gives rise to two distinct isoforms, lysosomal and secretory ASM (50). The lysosomal ASM resides in the endolysosomal compartment, whereas the secretory ASM is released by the secretory pathway and functions in the extracellular space.

In addition to indirect ASM inhibitors (desipramine), it has recently been discovered that several bisphosphonate compounds are selective direct inhibitors of ASM activity, including C10-BPA and zoledronic acid (48, 51). The most potent of the bisphosphonate derivatives, zoledronic acid (Reclast), an FDA-approved drug for the treatment of osteoporosis, exhibited IC_{50} of 20 nM toward ASM in vitro (51). To further investigate ASM involvement in glutamate-induced OL death, the direct inhibitors of ASM activity were employed (**Fig. 5A**). Reclast and C10-BPA significantly augmented OL survival in a concentration-dependent manner. In contrast, specific inhibitors of NSM activity, GW4869 and epoxyquinone G109 (52), did not have any effect, supporting the notion that ASM is essential for OL response to glutamate. To confirm our findings, ASM was knocked down using an RNAi approach. Figure 5B shows that knocking down ASM prevented OL demise in response to a broad range of glutamate concentrations. The data provide further evidence for a central role of the ASM-mediated mechanisms in governing OL response to glutamate toxicity. To determine whether glutamate treatment impacts ASM activity, OLs were exposed to 1 mM glutamate for a defined time, cells were harvested, and ASM or NSM activity was quantified. Figure 5C shows that glutamate triggered a sustained ASM activation for at least 8 h, whereas NSM activity did not change. There were no changes in the expression level of ASM protein in response to glutamate, indicating involvement of posttranscriptional mechanisms in ASM activation (Fig. 5D).

GSH is an upstream regulator of ASM activity

Glutamate-induced toxicity, which is mediated by competitive inhibition of system x_c^-, has been characterized as ferroptosis, an iron-, ROS-, and lipid peroxidation-mediated process (38). One metabolic consequence of system x_c^- inhibition is depletion of the intracellular cysteine pool, which is a precursor for GSH synthesis. In cancer cells, metabolic profiling revealed that GSH was dramatically
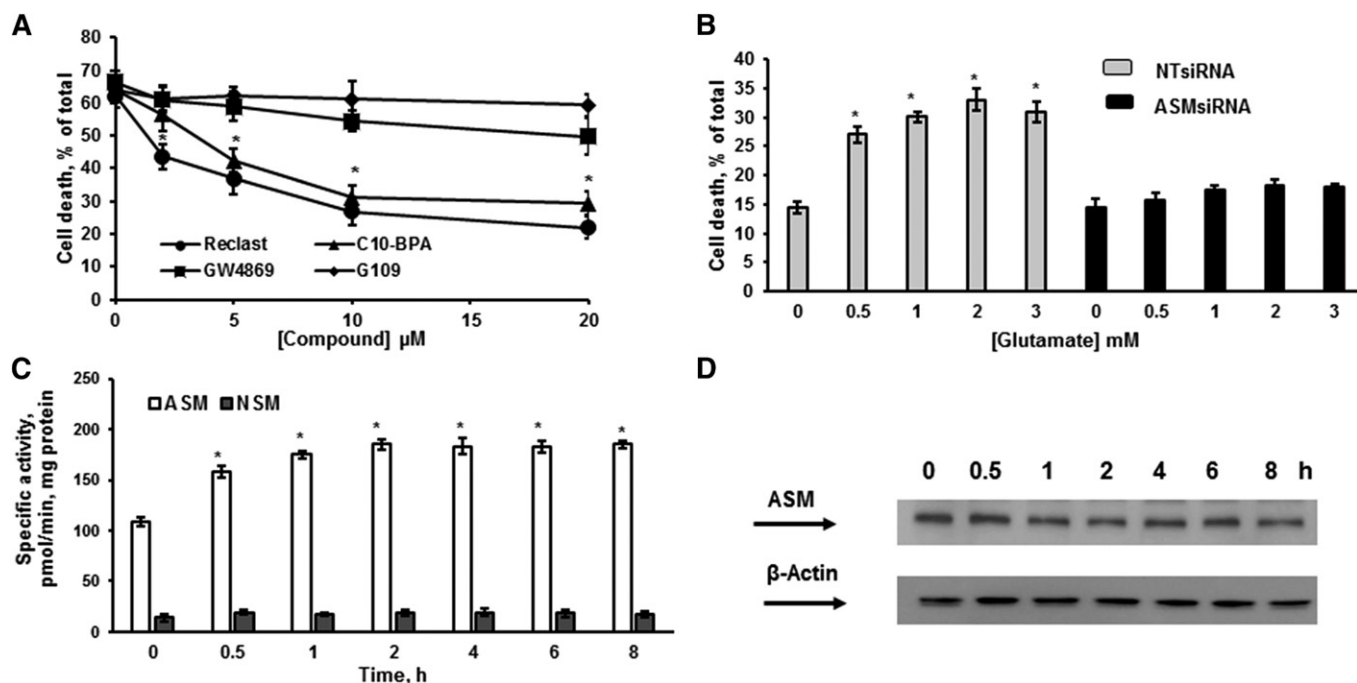
Fig. 5. ASM activation is critical for OL survival after glutamate treatment. A: OLs were treated with 1 mM glutamate with/without ASM (Reclast and C10-BPA) and NSM (GW4869 and epoxyquinone G109) inhibitors and relative cell survival was determined. Data are mean ± SE, *P < 0.05, n = 12. B: OLs were transfected with 20 nM of nontargeting siRNA pool (NT siRNA) or 20 nM of specific siRNA pool targeting different regions of the ASM gene (ASMsiRNA). Cells were plated and cultured for 24 h, then treated with 1 mM glutamate and relative cell survival was measured 24 h following glutamate treatment. Data are mean ± SE, *P < 0.05, n = 12. C. Time-course of specific ASM and NSM activity changes was determined following OL treatment with 1 mM glutamate. The enzyme activity is expressed as picomoles of C15-SM per minute per milligram protein. Data are mean ± SE, *P < 0.05, n = 12. D: The time-course of ASM protein expression changes was assessed following OL exposure to 1 mM glutamate. Cell lysates (30 µg/lane) were analyzed using anti-ASM antibody. To confirm equal loading of samples, the membranes were stripped and probed with anti-β-actin (Sigma-Aldrich) antibody. Data are representative of three independent experiments.

reduced during ferroptosis elicited by the system x_c^- inhibitor, erastin. This GSH depletion was sufficient for erastin-dependent cell death, as GSH depletion by another reagent, buthionine sulfoximine (BSO), also initiated ferroptosis (53). BSO is an inhibitor of glutamate-cysteine ligase, the rate-limiting enzyme for GSH synthesis. It has been demonstrated that GSH depletion results in the reduced activity of GSH-dependent enzymes, such as GSH peroxidases, leading to increased formation of lipid peroxides (3).

To investigate the mechanism of ASM activation, GSH content was determined in OLs after 6 h treatment with 1 mM glutamate. As expected, OL glutamate exposure significantly attenuated GSH content (**Fig. 6A**). Importantly, inhibiting ASM activity with Reclast (25 µM) did not have any effect on glutamate-induced depletion of GSH. The data suggest that ASM activation is an event that occurs downstream of GSH depletion in response to glutamate. To elucidate whether lowering the intracellular GSH is sufficient to activate the ASM, OLs were treated with 0.5 mM BSO for a defined time and the GSH content and ASM activity were measured. Figure 6B shows the reduced GSH content in OLs treated with BSO that was associated with augmented ASM activity (Fig. 6C). In contrast, lowering GSH content did not affect the NSM activity (Fig. 6C). The data suggest that glutamate-induced decline of the

intracellular GSH levels provoked a selective activation of the ASM and increased SM hydrolysis. To elucidate whether ASM is an upstream regulator of ROS generation and lipid peroxidation, the impact of ferroptosis inhibitors on glutamate-triggered ASM activation was measured in OLs (Fig. 6C). As expected, glutamate-induced ASM activation was prevented by 1 mM cystine. In contrast, CPX (5 µM) and ferrostatin-1 (5 µM) did not affect ASM activity, suggesting that ASM is an upstream regulator of ROS generation and lipid peroxidation in OL response to glutamate.

To confirm our findings, the sphingolipid profile was determined in cells treated with 1 mM glutamate with/without inhibitors. Figure 6E shows that glutamate treatment resulted in reduced SM content that was prevented by the ASM inhibitor, Reclast (25 µM), or by cystine (1 mM). In contrast, the lipid radical scavenger, Trolox (15 µM), the specific inhibitor of ferroptosis, ferrostatin-1 (5 µM), or the iron chelator, ciclopirox olamine (CPX) (5 µM), did not affect the SM decrease triggered by glutamate. Similarly, the glutamate-induced upregulation of SM hydrolysis products, sphingosine and ceramide, was prevented by cystine (1 mM) and Reclast (25 µM), but Trolox (15 µM), ferrostatin-1 (5 µM), and CPX (5 µM) did not have any effect (**Fig.7A**, B). The data support the notion that OL exposure to glutamate prompts a decline in
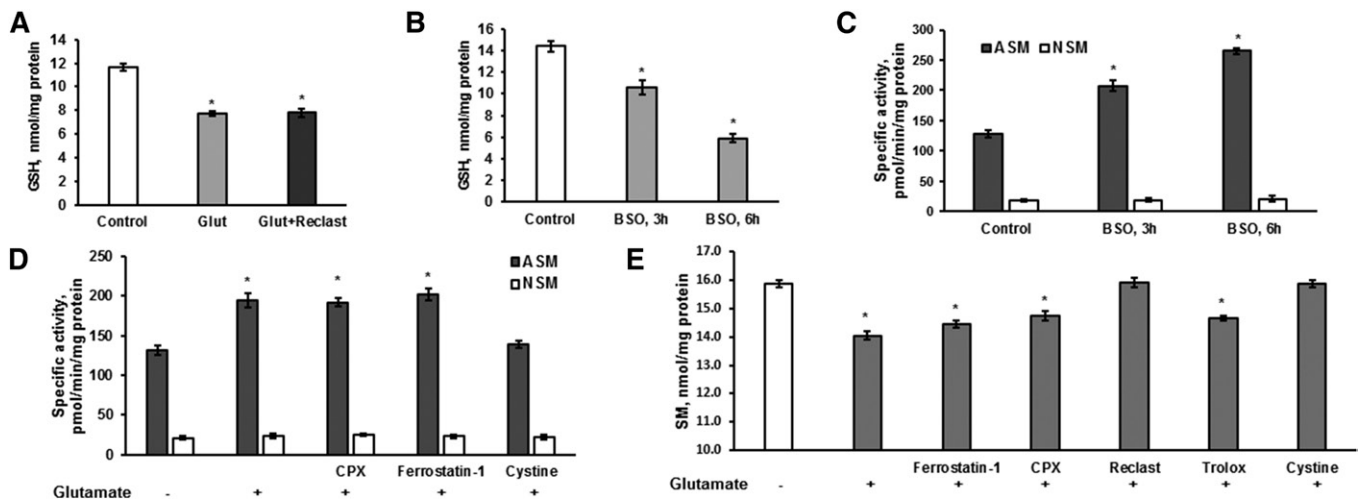
Fig. 6. ASM activation in response to glutamate is controlled by intracellular GSH in OLs. A: OLs were treated with 1 mM glutamate with/without the ASM inhibitor, Reclast (25 μM), for 6 h and GSH content was quantified. Data are mean ± SE, *$P < 0.05$, n = 8. B: OLs were exposed to 500 μM BSO and GSH content was determined. Data are mean ± SE, *$P < 0.05$, n = 8. C: OLs were treated with 500 μM BSO and specific ASM and NSM activity changes were determined. The enzyme activity is expressed as picomoles of C15-SM per minute per milligram protein. Data are mean ± SE, *$P < 0.05$, n = 12. D: OLs were exposed to 1 mM glutamate with/without the ferroptosis inhibitor, ferrostatin-1 (5 μM), the iron chelator, CPX (5 μM), or 1 mM cystine for 6 h. ASM and NSM specific activity was measured. The enzyme activity is expressed as picomoles of C15-SM per minute per milligram protein. Data are mean ± SE, *$P < 0.05$, n = 12. E: OLs were exposed to 1 mM glutamate with/without the ferroptosis inhibitor, ferrostatin-1 (5 μM), the iron chelator, CPX (5 μM), the radical scavenger, trolox (15 μM), the ASM inhibitor, Reclast (25 μM), or 1 mM cystine for 24 h. SM content changes were measured. Data are mean ± SE, *$P < 0.05$, n = 12. Each sample was normalized to its respective total protein levels.

GSH leading to activation of ASM and elevation of bioactive sphingolipids, which occur upstream of lipid peroxidation and the execution of regulated necrotic cell death.

Glutamate-elicited sphingosine accumulation is a cause of reduced respiratory chain maximal capacity

Having demonstrated that glutamate-triggered SM hydrolysis by ASM results in upregulation of sphingosine and
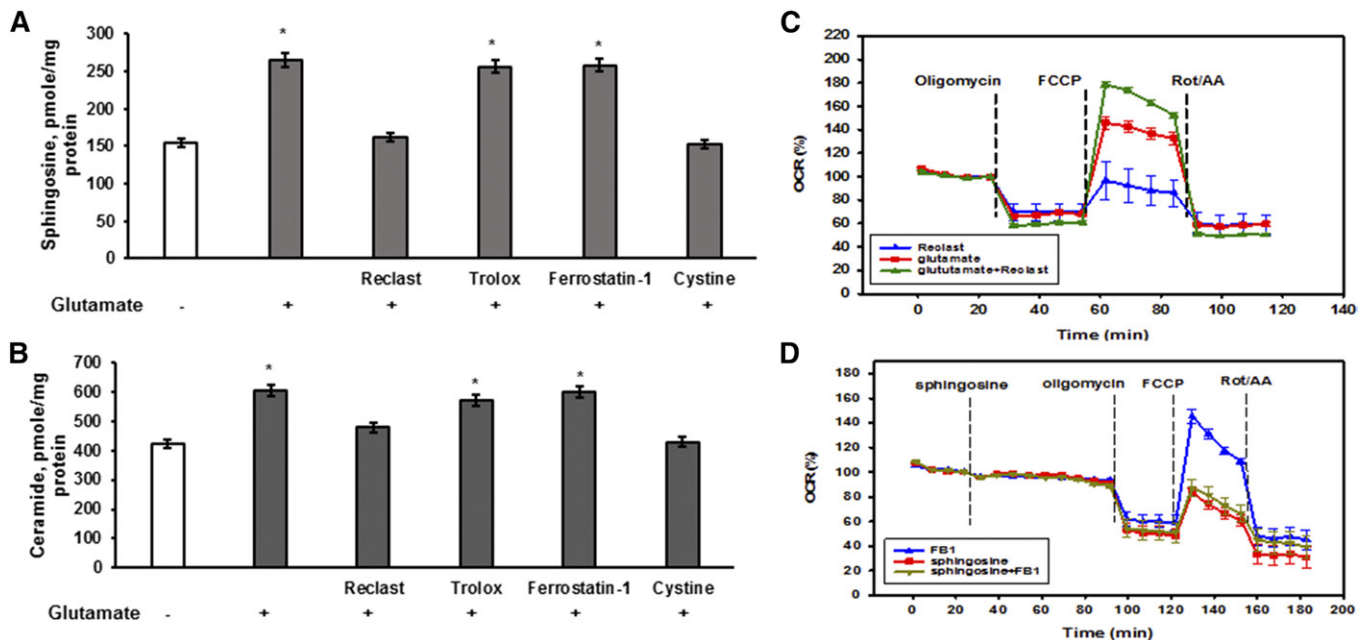
Fig. 7. ASM-dependent sphingosine accumulation mediates the inhibition of mitochondrial respiratory chain activity in OL response to glutamate. OLs were exposed to 1 mM glutamate with/without the ferroptosis inhibitor, ferrostatin-1 (5 μM), the iron chelator, CPX (5 μM), the radical scavenger, trolox (15 μM), the ASM inhibitor, Reclast (25 μM), or 1 mM cystine for 24 h. Sphingosine (A) and total ceramide (B) were measured. Data are mean ± SE, *$P < 0.05$, n = 12. Each sample was normalized to its respective total protein levels. C: OLs were treated with 1 mM glutamate for 6 h with/without 50 μM Reclast and the OCR was monitored. Data are representative of four independent experiments. D: OLs were treated with sphingosine or sphingosine with 50 μM FB1, a specific inhibitor of CerS activity, and the OCR was monitored. Data are representative of three independent experiments.

ceramide species (Figs. 5A, C and 7A, B), possibly in the ER and/or mitochondria, we investigated the potential downstream targets of bioactive sphingolipids. Experimental evidence implicates ceramide, which is elevated in cerebral mitochondria after brain IR, as a causal factor of mitochondrial defects (14, 15) leading to activation of apoptosis (17). In an animal model of TBI, a substantial increase of sphingosine levels in cerebral mitochondria has been shown to cause reduced activity of respiratory chain Complex IV (16). To determine the impact of glutamate-induced deregulation of sphingolipid metabolism in OLs, mitochondrial function was assessed using a Seahorse XF96 extracellular flux analyzer. Cells were exposed to 1 mM glutamate with/without 50 μM Reclast for 6 h and the OCR was monitored (Fig. 7C).

The OCR due to ATP production was determined by the addition of 1 μM oligomycin, an inhibitor of mitochondrial ATP-synthase. The oligomycin-sensitive OCR in OLs treated with glutamate or glutamate plus Reclast was similar to control. The addition of 2 μM carbonyl cyanide 4-(trifluoromethoxy)phenylhydrazone (FCCP), an uncoupler of oxidative phosphorylation, allows for the determination of the maximal OCR. Glutamate-treated OLs exhibited higher FCCP-dependent OCR compared with nontreated cells. This is consistent with a previous report showing that extracellular glutamate could be transported via system x $_c^-$ into OL cytosol, thereby increasing the availability of the substrates for oxidation in the mitochondrial respiratory chain (32). Importantly, the FCCP-stimulated OCR was further increased in OLs treated with glutamate plus Reclast (Fig. 7C), indicating that glutamate treatment caused the inhibition of the maximal OCR due to activation of ASM. The electron transport chain inhibitors, rotenone (Rot), a Complex I inhibitor, and antimycin A, a Complex III inhibitor, were added to inhibit mitochondrial respiration and assess the nonmitochondrial oxygen consumption. There were no changes in nonmitochondrial OCR between OLs treated with glutamate with/without Reclast and control cells. The data suggest that glutamate treatment resulted in reduced respiratory chain activity due to activation of ASM and SM hydrolysis leading to elevation of sphingosine and ceramide, which could inhibit the mitochondrial respiratory chain activity. Based on the pharmacological data analysis (Fig. 4D), ceramide involvement in the ASM-mediated inhibition of respiratory chain activity in OLs seems unlikely.

To investigate possible ASM-dependent sphingosine accumulation, mitochondria were isolated from OLs after exposure to 1 mM glutamate with/without 50 μM Reclast for 6 h and the sphingolipid profile was determined. Glutamate treatment resulted in a significant elevation of mitochondrial sphingosine up to 170% (78 ± 6.7 pmol/mg protein) compared with control (46 ± 4.9 pmol/mg protein) that was prevented by Reclast (49.9 ± 5.3 pmol/mg protein). There were no changes in mitochondrial ceramide levels following OLs' exposure to glutamate with/without Reclast.

To elucidate a causative role of glutamate-triggered sphingosine accumulation on mitochondrial respiratory chain activity, OLs were treated with 80 μM of exogenous sphingosine and mitochondrial function was analyzed. It has been previously reported that exogenous sphingosine could reach the mitochondrial compartment and affect mitochondrial function (18). Figure 7D shows that sphingosine did not affect the basal OCR, which agrees well with glutamate's lack of impact on basal respiration (Fig. 7C). The oligomycin-sensitive OCR in OLs treated with sphingosine was no different from control cells. Sphingosine significantly attenuated the FCCP-stimulated OCR, indicating the inhibition of the maximal respiratory chain activity. To rule out the possibility that sphingosine-induced inhibition of the maximal OCR could be due to ceramide generated by mitochondrial CerS using sphingosine as a substrate, OLs were exposed to 80 μM sphingosine with 50 μM FB1, a specific inhibitor of CerS activity. There was no impact of FB1 on the sphingosine-induced inhibition of FCCP-stimulated OCR, ruling out the ceramide involvement. The data suggest that glutamate-triggered activation of ASM and SM hydrolysis resulted in elevation of sphingosine, which attenuated the maximal mitochondrial respiratory chain activity.

Glutamate-triggered ASM activation and elevation of sphingosine leads to increased mitochondrial ROS

Multiple sources of ROS have been identified to promote lipid peroxidation, which is recognized as a central mechanism of ferroptosis (38). In addition to iron-mediated ROS production by Fenton reaction, NOX appears to be an important contributor to increased cellular ROS (12) in the erastin-induced ferroptosis in cancer cells, whereas the input of mitochondria-dependent ROS generation was negligible (13). Baseline mitochondria generate very low amounts of ROS, but ROS generation is profoundly increased in the presence of Complex I or III inhibitors (54). Having demonstrated ASM-dependent inhibition of the respiratory chain activity in response to glutamate, we sought to determine whether mitochondrial ROS are involved in facilitating the regulated necrosis in OLs. Cellular ROS generation was quantified using H2-DCF, which rapidly reacts with ROS to form dichlorofluorescein (DCF), a highly fluorescent compound. OLs were exposed to 1 mM glutamate with/without test compounds for 3 h and then H2-DCF dye was added and DCF fluorescence was measured (**Fig. 8A**). Glutamate stimulated cytosolic ROS generation that was prevented by 5 μM ferrostatin-1 or 1 μM PMC, indicating the engagement of ferroptotic oxidative mechanisms. Consistent with previous reports (13, 38), the NOX1/4 inhibitor, GKT137831 (15 μM), attenuated cellular ROS production. Both inhibitors of ASM activity, Reclast (25 μM) and desipramine (25 μM), significantly reduced cellular ROS generation in response to OL treatment with glutamate (Fig. 8A). The data suggest that ASM-dependent inhibition of respiratory chain activity resulted in the increased mitochondrial ROS generation that contributed to cellular ROS.

To elucidate the input of mitochondrial ROS in glutamate-dependent ferroptosis in OLs, mitochondrial ROS was measured using MitoSox Red fluorescent dye. OLs plated in a 96-well plate were exposed to 1 mM glutamate
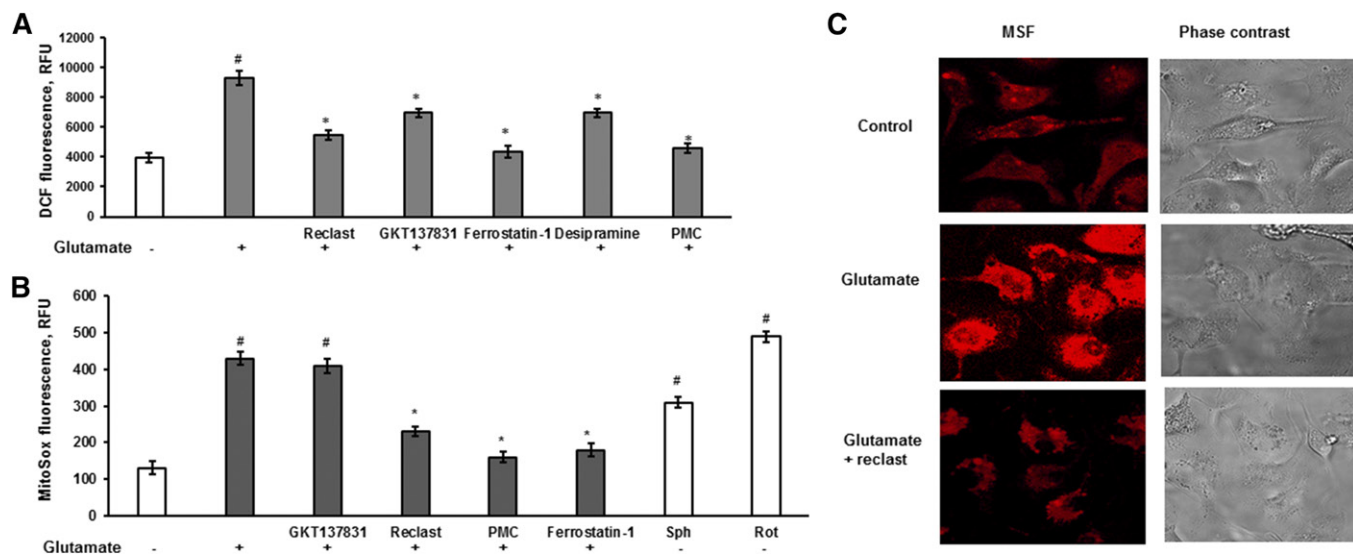
Fig. 8. ASM activation is necessary for glutamate-dependent cellular and mitochondrial ROS generation. A. OLs were treated with 1 mM glutamate with/without 25 μM Reclast, 25 μM desipramine, 5 μM ferrostatin-1, 1 μM PMC, or 15 μM GKT137831 for 3 h and DCF fluorescence was measured. Data are mean ± SE, *$P < 0.05$ compared with nontreated cells, #$P < 0.05$ compared with glutamate-treated cells, n = 12. B: Cells were exposed to 1 mM glutamate with/without 25 μM Reclast, 25 μM desipramine, 5 μM ferrostatin-1, 1 μM PMC, or 15 μM GKT137831 for 3 h and MitoSox fluorescence was measured. Control cells were treated with either 25 μM sphingosine or 1 μM Rot as a positive control. #$P < 0.05$ compared with nontreated cells, *$P < 0.05$ compared with glutamate-treated cells, n = 12. C: OLs were treated with 1 mM glutamate with/without 25 μM Reclast for 3 h and MitoSox fluorescence (MSF) as well as phase contrast images were captured using confocal microscopy.

with/without inhibitors for 3 h or treated with 5 μM Rot, a mitochondrial Complex I inhibitor, or 50 μM sphingosine. Cells were washed with DPBS buffer and then incubated with 5 μM MitoSox Red in DPBS buffer for 10 min at 37°C to allow the dye to reach mitochondria. Cells were washed to remove the excess of dye and the MitoSox fluorescence was determined in the plate-reader. Figure 8B shows that glutamate treatment augmented mitochondrial ROS production in OLs similar to the Complex I inhibitor, Rot, which was used as a positive control. Glutamate-triggered MitoSox fluorescence was sensitive to the ferroptosis inhibitors, ferrostatin-1 (5 μM) and PMC (1 μM), indicating that mitochondrial ROS generation contributes to ferroptosis in OLs. In contrast, the NOX1/4 inhibitor, GKT137831 (15 μM), did not affect the MitoSox fluorescence response. Of note, the glutamate-induced mitochondrial ROS generation was attenuated by the ASM inhibitor, Reclast (25μM), which suggests ASM participation in facilitating the mitochondrial ROS generation. Consistent with its ability to inhibit the mitochondrial respiratory chain function (Fig. 7D), sphingosine augmented mitochondrial ROS production (Fig. 8B). Furthermore, the MitoSox fluorescence response in OLs was visualized using confocal microscopy. Glutamate (1 mM) enhanced mitochondrial ROS generation, which was attenuated by 25 μM Reclast (Fig. 8C). The data suggest that ASM-dependent mitochondrial ROS generation is an important contributing factor to glutamate-induced regulated necrosis in OLs.

Glutamate-induced MPTP opening is required for promoting regulated necrosis in OLs

The mitochondrial permeability transition pore (MPTP), a high-conductance channel in the inner mitochondrial membrane, serves as a switch between apoptosis and necrosis. Cell death proceeds through necrosis when the MPTP opens causing dissipation of the transmembrane potential and an inhibition of ATP production. If the MPTP does not open, cellular ATP can be maintained to support the energy demand of apoptosis (55). MPTP opening due to Ca^{2+} overload and increased ROS causes dissipation of transmembrane potential, ATP hydrolysis, Ca^{2+} release, pyridine nucleotide depletion, and matrix swelling, which results in outer membrane rupture (56). MPTP forms from the F-ATP synthase and cyclophilin D (CypD) binding to the oligomycin sensitivity-conferring protein (OSCP) subunit of F-ATP synthase regulates the channel activity (57). CypD sensitizes MPTP to Ca^{2+} and confers sensitivity to cyclosporin A (CSA), but is not an essential pore component (55, 58). A chief mitochondrial deacetylase, SIRT3, has been shown to deacetylate CypD, diminishing its peptidyl-prolyl *cis-trans* isomerase activity and leading to suppression of the MPTP opening (59). Moreover, SIRT3 has been implicated in strengthening the cellular antioxidant defense by deacetylating mitochondrial SOD2, which increases its ROS scavenging activity (60).

To determine the possible role of MPTP opening in glutamate-induced ASM-dependent regulated necrosis, the mitochondrial transmembrane potential changes that are indicative of MPTP opening were analyzed (61). OLs were treated with 1 mM glutamate for 18 h with/without Reclast (25 μM). Cells were washed and loaded with TRMR fluorescent dye, which is sensitive to mitochondrial transmembrane potential. TRMR fluorescence was attenuated by glutamate treatment (**Fig. 9A**); however, Reclast prevented the glutamate-induced decrease in the mitochondrial transmembrane potential, suggesting that glutamate-induced activation of
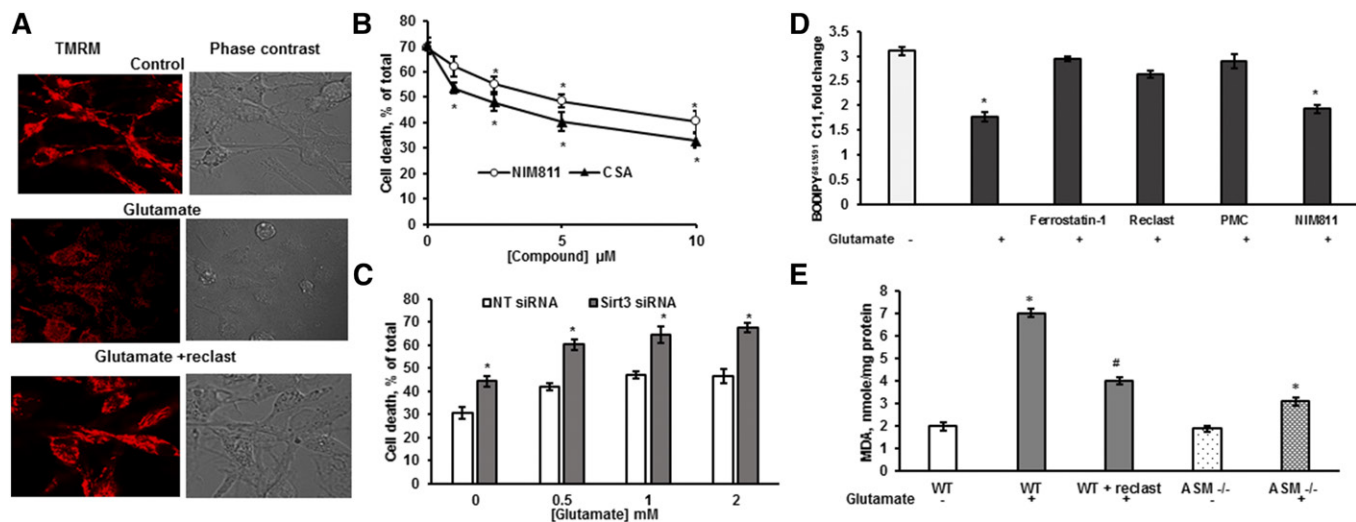
Fig. 9. ASM is essential for glutamate-induced MPTP opening and activation of lipid peroxidation. A: Cells were exposed to 1 mM gluta- mate with/without 25 μM Reclast for 18 h, then loaded with TMRM, and the TMRM fluorescence as well as phase contrast images were captured using confocal microscopy. B: Cells were exposed to 1 mM glutamate with/without CSA or NIM811 and cell survival was quantified 24 h later. Data are mean ± SE, *$P < 0.05$, n = 12. C: OLs were transfected with 20 nM of nontargeting siRNA pool (NT siRNA) or 20 nM of specific siRNA pool targeting the Sirt3 gene (Sirt3 siRNA). Cells were cultured for 24 h, then treated with glutamate, and relative cell survival was measured 24 h later. Data are mean ± SE, *$P < 0.05$, n = 12. D: OLs were exposed to 1 mM glutamate with/without 5 μM ferrostatin-1, 25 μM Reclast, 1 μM PMC, or 10 μM NIM811 for 24 h and the ratio of BODIPY$^{581/591}$ C11 fluorescence shift was quantified. Data are mean ± SE, *$P < 0.05$, n = 8. E: OLs were isolated from WT mice (WT) or from ASM-deficient mice (ASM$^{-/-}$) were treated with 1 mM glutamate for 24 h. WT cells were treated with 1 mM glutamate with 25 μM Reclast. MDA content was measured. Data are mean ± SE, *$P < 0.05$ compared with nontreated cells, # $P < 0.05$ compared with glutamate-treated cells, n = 12.

ASM resulted in dissipation of transmembrane potential, most likely due to MPTP opening. To determine whether MPTP opening is necessary for glutamate-induced regulated necrosis in OLs, the effect of MPTP inhibitors on OL survival was quantified. Figure 9B shows that NIM811, a highly selec- tive MPTP inhibitor (62), as well as CSA, a potent MPTP inhibitor, significantly improved OL survival in response to glutamate. The data support the notion that glutamate- triggered activation of ASM and sphingosine accumulation stimulated ROS generation, leading to MPTP opening and dissipation of mitochondrial transmembrane potential.

To elucidate a possible input of SIRT3 in regulating glu- tamate-induced cell death, Sirt3 gene expression was knocked down with 20 nM siRNA pool targeting four dif- ferent regions of the gene to minimize the off-target effects. Figure 9C shows that knocking down SIRT3 sig- nificantly augmented OL demise. The data indicate the protective role of SIRT3 in glutamate-triggered regulated necrotic cell death.

Glutamate-induced lipid peroxidation was attenuated by hindering ASM

Lipid peroxidation seems to be a fundamental mecha- nism of ferroptotic cell death (38). Therefore, lipophilic antioxidants and radical scavengers, including ferro- statin-1, liproxstatin-1, and PMC, are potent inhibitors of ferroptosis (39). To further investigate the mechanism of ASM participation in glutamate-induced regulated necrosis, the oxidation of cellular lipids was analyzed. Lipid peroxi- dation was measured in live cells using BODIPY$^{581/591}$ C11,

an intrinsically lipophilic fluorophore. Upon oxidation of the polyunsaturated butadienyl portion of the dye, the fluorescence emission peak shifts from 590 nm to 510 nm, providing a basis for ratio-fluorescence quantitation of lipid peroxidation (63). OLs were plated in a 96-well plate and treated with 1 mM glutamate with/without inhibitors for 18 h and incubated with 10 μM BODIPY$^{581/591}$ C11 for 30 min. After medium removal and thorough cell washing, the fluorescence shift was measured (Fig. 9D). Glutamate treatment augmented lipid peroxide production, which was prevented by 1 μM ferrostatin-1 or 5 μM PMC. The ASM inhibitor, Reclast (25 μM), significantly reduced glu- tamate-initiated lipid peroxidation, indicating the promi- nent role of the ASM-mediated pathway in lipid ROS production. There was no effect of NIM811 (10 μM) on glutamate-induced lipid peroxidation, supporting the notion that the MPTP is a downstream target of glutamate-trig- gered ROS, which is in line with the well-known sensitivity of MPTP to oxidative stress (64). It also shows that, in con- trast to the generally accepted view concerning uncon- trolled lipid peroxidation as a final step in the execution of ferroptosis, the final step in ferroptosis-like cell death in OLs is a bioenergetic catastrophe precipitated by MPTP opening. Furthermore, the end product of lipid peroxida- tion, MDA, was measured following 1 mM glutamate expo- sure for 18 h in OLs isolated from WT mouse brains and ASM-deficient mouse brains. Figure 9E shows that gluta- mate triggered an MDA increase in WT cells, but not in OLs isolated from ASM-deficient mice. The glutamate- induced MDA was significantly attenuated by the ASM

inhibitor, Reclast, in WT OLs. The data suggest that the ASM-dependent pathway contributes to glutamate-induced ROS generation and lipid peroxidation in OLs.

DISCUSSION

These studies provide evidence for a novel ASM-dependent mechanism furthering mitochondrial dysfunction and regulated necrosis following OL treatment with glutamate. Our data suggest that glutamate-triggered decline of intracellular GSH results in the activation of ASM and upregulation of sphingosine, which, in turn, inhibits the mitochondrial respiratory chain, leading to generation of ROS, opening of the MPTP, and necrotic cell death.

Our studies provide the experimental evidence supporting the important role of system x_c^--dependent regulated necrosis in OL response to glutamate. Here, we show that glutamate-induced OL demise is prevented by cystine (Fig. 1A), indicating system x_c^- involvement. Glutamate toxicity is not sensitive to pan-caspase inhibitor and lacks the activation of executioner caspase 3/7 in OLs (Fig. 1B, C). We have previously reported that OL exposure to glutamate in cystine-containing medium resulted in activation of a caspase 3/7 and Ca^{2+}-dependent apoptotic mechanism of OL demise (31). In these studies, OLs were isolated using the previous protocol, but treated with glutamate in cystine-free medium. Lack of caspase 3/7 activation and Ca^{2+} involvement in OL death following treatment with glutamate in cystine-free medium (Fig. 1C) implicates cystine as a prominent factor controlling the mechanism of glutamate-dependent OL death. OLs express ionotropic glutamate receptors, including AMPA/kainate and NMDA receptors throughout their lineage (65). Glutamate interaction with OLs could occur through the ionotropic glutamate receptors and/or glutamate/cystine antiporter (38). While cystine is present in the OL culture medium, the glutamate/cystine antiporter seems to be able to maintain intracellular GSH levels, and glutamate binding to ionotropic glutamate receptors results in Ca^{2+} influx into the cytosol leading to increased mitochondrial Ca^{2+} uptake, calpain activation, and apoptotic cell death. When OLs were exposed to glutamate in the absence of cystine, decreased cystine import triggered GSH depletion leading to system x_c^--dependent regulated necrotic cell death.

Importantly, glutamate-triggered response is not sensitive to the selective necroptosis inhibitor, necrostatin-1s; however, its derivative, necrostatin-1, augmented OL survival (Fig. 1D). Further investigation of the necroptotic signaling mechanisms, including RIPK1- and RIPK3-mediated formation of necrosome, ruled out necroptosis involvement in glutamate-induced OL death (Fig. 2A, B). The data suggest that the protective effect of necrostatin-1 is not mediated by its conventional target, RIPK1, a driving force of necroptotic cell death. Both necrostatin-1 and necrostatin-1s seemed to reduce the infarct size in the experimental stroke model, which was interpreted as an indication of RIPK1-mediated necroptotic cell death following cerebral IR (2). Of note, necrostatin-1 did not have any effect on ASM activity (not shown); therefore, the necrostatin-1-mediated protection of OLs against glutamate toxicity is not attributed to ASM inhibition. The data suggest that necrostatin-1 protected brain from IR via an unknown target, which is not a part of the necroptotic signaling mechanism. Moreover, it has been reported that autophagy is an essential mechanism of erastin-induced ferroptosis in cancer cells (66); however, our data indicate a lack of autophagic mechanism activation in glutamate-induced toxicity of OLs (Fig. 2C).

Cerebral IR affects both neurons and OLs; however, less is known about the mechanisms of OL injury. Clinical trial outcomes for neuroprotective drugs in stroke have been disappointing, partly due to the drugs' failure to ameliorate the damage to OLs (67). Importantly, OL impairment could trigger a secondary injury to neurons (68). These studies are the first detailed investigation of the mechanisms of system x_c^--dependent regulated necrotic cell death in primary OLs. Pharmacologic inhibitor profiling revealed ferroptosis as a key mechanism of glutamate-initiated regulated necrotic cell death in OLs (Fig. 3). Thus, specific inhibitors of ferroptosis (ferrostatin-1 and liproxstatin-1), antioxidants (NAC, PMC, mitoTEMPO, and trolox), inhibitors of key enzymes promoting lipid peroxidation, such as lipoxygenase and NOX (LOXBlock-1, zileuton, apocynin, and GKT137831), and iron chelators (DFA and CPX) augmented OL survival. The pharmacologic analysis data are consistent with the reports characterizing the well-established ferroptotic cell death mechanisms in various cell types (1, 13, 38), implying ferroptosis as the central mechanism of glutamate-induced OL demise. The biological significance of ferroptosis is expanding rapidly by virtue of the discovery that system x_c^- is a crucial regulator of ferroptosis as well as the use ferrostatin-1 to inhibit ferroptosis in diverse in vivo models of disease. The results of these studies are in line with emerging evidence of the important role of ferroptosis in mouse models of IR injury. Thus, liver or kidney IR injury can be ameliorated by the ferroptosis inhibitor, ferrostatin-1 (12); however, the relevance of ferroptosis in stroke and TBI remains to be established.

These studies point to an important role of sphingolipids and sphingolipid-metabolizing enzymes in the glutamate-induced OL response. Here, we show that bioactive sphingolipids (ceramide and sphingosine) are upregulated, while SM is reduced (Fig. 4A–C), suggesting an activation of SM hydrolysis, not the activation of sphingolipid biosynthesis. Indeed, specific inhibitors of the lysosomal pathway of SM degradation (desipramine and LCL-521) attenuated OL cell death, while inhibitors of de novo sphingolipid biosynthesis (myriocin and FB1) did not. Furthermore, our studies identified ASM as a novel critical factor in ferroptotic cell death and provide further insight into sphingolipid-mediated mechanisms of OL injury. Thus, direct functional inhibitors of ASM activity, Reclast and C10-BPA, as well as knocking down ASM using RNAi augmented OL survival (Fig. 5A, B). Our studies demonstrate that glutamate triggered the selective activation of ASM, not NSM, via posttranslational mechanisms (Fig. 5C, D).

Here, we show that glutamate-induced decline of intracellular GSH results in a selective increase of ASM activity (Fig. 6A–C) that is independent of ROS generation and lipid peroxidation (Fig. 6D, E).

Different activation mechanisms of ASM have been described in response to cellular stress induced by cytokines, radiation, and chemotherapeutic agents (69, 70). It has been reported that PKCδ-mediated phosphorylation of a specific serine residue on ASM (Ser508) is indispensable for its activation in response to UV irradiation or treatment with phorbol ester PMA (71, 72). Recently, activation of PKCδ has been demonstrated in cell response to GSH depletion by BSO (73). It is conceivable that ASM could be activated by PKCδ-dependent phosphorylation in response to glutamate-induced GSH depletion in OLs. Another potential posttranslational mechanism regulating ASM activity could be S-glutathionylation. A reversible protein cysteine sulfhydryl moiety modification by glutathionylation has emerged as an essential mechanism of posttranslational protein modification in conditions associated with oxidative or nitrosative stress (IR) and inflammation (74). A large number of proteins have been reported to be modified by S-glutathionylation leading to change in the catalytic or structural properties of proteins. In some cases, S-glutathionylation has been reported to be a mechanism for maintaining proteins in an inactive state, causing them to remain dormant until activated by well-regulated deglutathionylation reactions (75). Of note, ASM enzyme activity can be modulated by the deletion or chemical modification of a free C-terminal cysteine (Cys629), which is involved in the active site zinc coordination (76). However, these hypothetical mechanisms of GSH-dependent regulation of ASM activity certainly require further investigation.

Having shown the GSH-dependent ASM activation in response to glutamate, we investigated the potential targets of bioactive sphingolipids (ceramide and sphingosine) that accumulated in OLs as a result of enhanced ASM activity (Fig. 7A, B). Our studies indicate that glutamate treatment reduced the maximal capacity of the mitochondrial respiratory chain, which was rescued by inhibiting ASM with Reclast (Fig. 7C). Of note, sphingosine was able to mimic the glutamate-induced respiratory chain defect, suggesting that ASM-generated sphingosine targets the mitochondria and promotes mitochondrial dysfunction (Fig. 7D). These data further support the concept that ASM-dependent generation of both ceramide and sphingosine occurs in lysosomes, but only sphingosine can leave the lysosomal compartment and impact mitochondria (77).

These studies draw attention to a novel mechanism of endolysosomal ASM/sphingosine system involvement in promoting cell death. It is important to emphasize that ASM functions in the endolysosomal compartment and on the outer leaflet of the plasma membrane (78). In wounded cells, Ca^{2+} influx induces exocytosis of lysosomes and association of ASM with the plasma membrane, where the enzyme triggers ceramide-mediated invagination of the damaged plasma membrane to facilitate endocytosis and damage repair (79). Numerous studies demonstrated a pivotal role of ASM/ceramide in apoptosis induced by various stimuli (e.g., TNF-α, INF-γ, etoposide, radiation, etc.) (45, 80). Upon certain stimuli, ASM translocates from the lysosomes to the outer leaflet of the plasma membrane where ASM-generated ceramide leads to formation of ceramide-enriched membrane platforms that are central for apoptotic signal transduction (69, 81). This study is the first demonstration of lysosomal ASM/sphingosine involvement in perturbing mitochondrial function that results in regulated necrotic cell death.

Our studies extend the experimental evidence of a prominent role of ROS in system x$_c^-$-dependent regulated necrosis and highlight the contribution of the ASM-dependent pathway of cellular ROS generation in OLs (Fig. 8A). Several sources of ROS have been found to be important to the induction of ferroptosis in response to erastin-mediated inhibition of system x$_c^-$, including NOX, the iron-dependent Fenton reaction, lipoxygenase, and lipid ROS generation due to inactivation of glutathione peroxidase 4 (12). In cancer cells, there was no change in mitochondrial ROS in response to system x$_c^-$ inhibition with erastin; therefore, mitochondrial respiratory chain-mediated ROS contribution in ferroptosis was ruled out (13). The results of our studies identify a novel pathway in system x$_c^-$-dependent regulated necrosis and point to the critical role of ASM as a facilitator of sphingosine generation leading to inhibition of the mitochondrial respiratory chain and increased mitochondrial ROS in OLs (Fig. 8B, C). It appears that ferroptosis is produced by a dynamic interplay of multiple ROS-generating cascades, emphasizing the importance of defining the stimulus- and cell type-specific context.

The experimental evidence implicates the ASM/sphingosine system as an upstream regulator of MPTP opening in the neural cell response to glutamate, which is a major contributing factor to cell death following cerebral IR or TBI. The data are consistent with the previously established role of MPTP opening as a cause of the neural cell demise by necrosis in the infarct core after stroke, while it remains closed during apoptotic cell death in the penumbra (55). Of note, ASM-deficient mice exhibited a reduced infarct size after transient cerebral IR; however, the detailed mechanisms were not elucidated (19). Overall, these studies reveal ASM as a novel determinant of mitochondrial dysfunction in glutamate-induced regulated necrosis, which could be important to brain injury after cerebral IR.

The critical impact of SIRT3 in OL survival response to glutamate (Fig. 9C) is in line with SIRT3 participation in the cellular antioxidant defense system (82). Thus, SIRT3 deacetylates hepatic SOD2, a mitochondrial antioxidant enzyme, enhancing its ability to scavenge ROS in response to caloric restriction (60). In addition, SIRT3 activates an isocitrate dehydrogenase 2, a tricarboxylic acid cycle enzyme producing NADPH, due to caloric restriction, which results in increased activity of glutathione reductase and augmented generation of GSH, a major cellular antioxidant (83). Moreover, SIRT3 has been shown to deacetylate CypD leading to suppression of the MPTP opening in mitochondria, which diminished cell injury in aging (59). Our studies further support the concept that SIRT3-mediated

deacetylation pursues its target in a stimuli-specific manner (84). Recently, we described the pivotal role of SIRT3 in promoting CerS/ceramide-mediated mitochondrial injury, leading to apoptosis in response to cerebral IR. In contrast, these studies underscore the protective role of SIRT3 in glutamate-induced ASM/sphingosine-mediated mitochondrial dysfunction leading to necrotic cell death. The evidence suggests that SIRT3 is a pleiotropic gene that functions in a stimuli- and target substrate-specific manner to control multiple regulated cell death pathways.

In summary, the results of these studies highlight a novel mechanism of ASM involvement in governing mitochondrial respiratory chain-dependent ROS generation and suggest an important role of ASM in glutamate-induced regulated necrosis in the brain.▪

REFERENCES

1. Conrad, M., J. P. Angeli, P. Vandenabeele, and B. R. Stockwell. 2016. Regulated necrosis: disease relevance and therapeutic opportunities. *Nat. Rev. Drug Discov.* **15:** 348–366.
2. Degterev, A., Z. Huang, M. Boyce, Y. Li, P. Jagtap, N. Mizushima, G. D. Cuny, T. J. Mitchison, M. A. Moskowitz, and J. Yuan. 2005. Chemical inhibitor of nonapoptotic cell death with therapeutic potential for ischemic brain injury. *Nat. Chem. Biol.* **1:** 112–119.
3. Friedmann Angeli, J. P., M. Schneider, B. Proneth, Y. Y. Tyurina, V. A. Tyurin, V. J. Hammond, N. Herbach, M. Aichler, A. Walch, E. Eggenhofer, et al. 2014. Inactivation of the ferroptosis regulator Gpx4 triggers acute renal failure in mice. *Nat. Cell Biol.* **16:** 1180–1191.
4. Benveniste, H., J. Drejer, A. Schousboe, and N. Diemer. 1984. Elevation of extracellular concentrations of glutamate and aspartate in rat hippocampus during transient cerebral ischemia monitored by intracerebral microdialysis. *J. Neurochem.* **43:** 1369–1374.
5. Guerriero, R. M., C. C. Giza, and A. Rotenberg. 2015. Glutamate and GABA imbalance following traumatic brain injury. *Curr. Neurol. Neurosci. Rep.* **15:** 27.
6. Matute, C., M. Domercq, and M. V. Sanchez-Gomez. 2006. Glutamate-mediated glial injury: mechanisms and clinical importance. *Glia.* **53:** 212–224.
7. Rosin, C., T. E. Bates, and S. D. Skaper. 2004. Excitatory amino acid induced oligodendrocyte cell death in vitro: receptor-dependent and -independent mechanisms. *J. Neurochem.* **90:** 1173–1185.
8. Murphy, T. H., M. Miyamoto, A. Sastre, R. L. Schnaar, and J. T. Coyle. 1989. Glutamate toxicity in a neuronal cell line involves inhibition of cystine transport leading to oxidative stress. *Neuron.* **2:** 1547–1558.
9. Bridges, R. J., N. R. Natale, and S. A. Patel. 2012. System xc(-) cystine/glutamate antiporter: an update on molecular pharmacology and roles within the CNS. *Br. J. Pharmacol.* **165:** 20–34.
10. Albrecht, P., J. Lewerenz, S. Dittmer, R. Noack, P. Maher, and A. Methner. 2010. Mechanisms of oxidative glutamate toxicity: the glutamate/cystine antiporter system xc- as a neuroprotective drug target. *CNS Neurol. Disord. Drug Targets.* **9:** 373–382.
11. Lewerenz, J., S. J. Hewett, Y. Huang, M. Lambros, P. W. Gout, P. W. Kalivas, A. Massie, I. Smolders, A. Methner, M. Pergande, et al. 2013. The cystine/glutamate antiporter system x(c) (-) in health and disease: from molecular mechanisms to novel therapeutic opportunities. *Antioxid. Redox Signal.* **18:** 522–555.
12. Xie, Y., W. Hou, X. Song, Y. Yu, J. Huang, X. Sun, R. Kang, and D. Tang. 2016. Ferroptosis: process and function. *Cell Death Differ.* **23:** 369–379.
13. Dixon, S. J., K. M. Lemberg, M. R. Lamprecht, R. Skouta, E. M. Zaitsev, C. E. Gleason, D. N. Patel, A. J. Bauer, A. M. Cantley, W. S. Yang, et al. 2012. Ferroptosis: an iron-dependent form of nonapoptotic cell death. *Cell.* **149:** 1060–1072.
14. Yu, J., S. A. Novgorodov, D. Chudakova, H. Zhu, A. Bielawska, J. Bielawski, L. M. Obeid, M. S. Kindy, and T. I. Gudz. 2007. JNK3 signaling pathway activates ceramide synthase leading to mitochondrial dysfunction. *J. Biol. Chem.* **282:** 25940–25949.
15. Novgorodov, S. A., and T. I. Gudz. 2011. Ceramide and mitochondria in ischemic brain injury. *Int. J. Biochem. Mol. Biol.* **2:** 347–361.
16. Novgorodov, S. A., C. L. Riley, J. Yu, K. T. Borg, Y. A. Hannun, R. L. Proia, M. S. Kindy, and T. I. Gudz. 2014. Essential roles of neutral ceramidase and sphingosine in mitochondrial dysfunction due to traumatic brain injury. *J. Biol. Chem.* **289:** 13142–13154.
17. Novgorodov, S. A., C. L. Riley, J. A. Keffler, J. Yu, M. S. Kindy, W. B. Macklin, D. B. Lombard, and T. I. Gudz. 2016. SIRT3 deacetylates ceramide synthases: implications for mitochondrial dysfunction and brain injury. *J. Biol. Chem.* **291:** 1957–1973.
18. Zigdon, H., A. Kogot-Levin, J. W. Park, R. Goldschmidt, S. Kelly, A. H. Merrill, Jr., A. Scherz, Y. Pewzner-Jung, A. Saada, and A. H. Futerman. 2013. Ablation of ceramide synthase 2 causes chronic oxidative stress due to disruption of the mitochondrial respiratory chain. *J. Biol. Chem.* **288:** 4947–4956.
19. Yu, Z. F., M. Nikolova-Karakashian, D. Zhou, G. Cheng, E. H. Schuchman, and M. P. Mattson. 2000. Pivotal role for acidic sphingomyelinase in cerebral ischemia-induced ceramide and cytokine production, and neuronal apoptosis. *J. Mol. Neurosci.* **15:** 85–97.
20. Herr, I., A. Martin-Villalba, E. Kurz, P. Roncaioli, J. Schenkel, M. G. Cifone, and K. M. Debatin. 1999. FK506 prevents stroke-induced generation of ceramide and apoptosis signaling. *Brain Res.* **826:** 210–219.
21. Ohtani, R., H. Tomimoto, T. Kondo, H. Wakita, I. Akiguchi, H. Shibasaki, and T. Okazaki. 2004. Upregulation of ceramide and its regulating mechanism in a rat model of chronic cerebral ischemia. *Brain Res.* **1023:** 31–40.
22. Henry, B., R. Ziobro, K. A. Becker, R. Kolesnick, and E. Gulbins. 2013. Acid sphingomyelinase. *Handb. Exp. Pharmacol.* **215:** 77–88.
23. Gulbins, E., M. Palmada, M. Reichel, A. Luth, C. Bohmer, D. Amato, C. P. Muller, C. H. Tischbirek, T. W. Groemer, G. Tabatabai, et al. 2013. Acid sphingomyelinase-ceramide system mediates effects of antidepressant drugs. *Nat. Med.* **19:** 934–938.
24. Lee, J. K., H. K. Jin, M. H. Park, B. R. Kim, P. H. Lee, H. Nakauchi, J. E. Carter, X. He, E. H. Schuchman, and J. S. Bae. 2014. Acid sphingomyelinase modulates the autophagic process by controlling lysosomal biogenesis in Alzheimer's disease. *J. Exp. Med.* **211:** 1551–1570.
25. Horinouchi, K., S. Erlich, D. P. Perl, K. Ferlinz, C. L. Bisgaier, K. Sandhoff, R. J. Desnick, C. L. Stewart, and E. H. Schuchman. 1995. Acid sphingomyelinase deficient mice: a model of types A and B Niemann-Pick disease. *Nat. Genet.* **10:** 288–293.
26. Chudakova, D. A., Y. H. Zeidan, B. W. Wheeler, J. Yu, S. A. Novgorodov, M. S. Kindy, Y. A. Hannun, and T. I. Gudz. 2008. Integrin-associated Lyn kinase promotes cell survival by suppressing acid sphingomyelinase activity. *J. Biol. Chem.* **283:** 28806–28816.
27. Panov, A. V., S. Lund, and J. T. Greenamyre. 2005. Ca2+-induced permeability transition in human lymphoblastoid cell mitochondria from normal and Huntington's disease individuals. *Mol. Cell. Biochem.* **269:** 143–152.
28. Gerencser, A. A., A. Neilson, S. W. Choi, U. Edman, N. Yadava, R. J. Oh, D. A. Ferrick, D. G. Nicholls, and M. D. Brand. 2009. Quantitative microplate-based respirometry with correction for oxygen diffusion. *Anal. Chem.* **81:** 6868–6878.
29. Maldonado, E. N., D. N. DeHart, J. Patnaik, S. C. Klatt, M. B. Gooz, and J. J. Lemasters. 2016. ATP/ADP turnover and import of glycolytic ATP into mitochondria in cancer cells is independent of the adenine nucleotide translocator. *J. Biol. Chem.* **291:** 19642–19650.
30. Novgorodov, A. S., M. El-Alwani, J. Bielawski, L. M. Obeid, and T. I. Gudz. 2007. Activation of sphingosine-1-phosphate receptor S1P5 inhibits oligodendrocyte progenitor migration. *FASEB J.* **21:** 1503–1514.
31. Novgorodov, S. A., D. A. Chudakova, B. W. Wheeler, J. Bielawski, M. S. Kindy, L. M. Obeid, and T. I. Gudz. 2011. Developmentally regulated ceramide synthase 6 increases mitochondrial Ca2+ loading capacity and promotes apoptosis. *J. Biol. Chem.* **286:** 4644–4658.
32. Oka, A., M. J. Belliveau, P. A. Rosenberg, and J. J. Volpe. 1993. Vulnerability of oligodendroglia to glutamate: pharmacology, mechanisms, and prevention. *J. Neurosci.* **13:** 1441–1453.
33. Tait, S. W., G. Ichim, and D. R. Green. 2014. Die another way–nonapoptotic mechanisms of cell death. *J. Cell Sci.* **127:** 2135–2144.

34. Murphy, J. M., P. E. Czabotar, J. M. Hildebrand, I. S. Lucet, J. G. Zhang, S. Alvarez-Diaz, R. Lewis, N. Lalaoui, D. Metcalf, A. I. Webb, et al. 2013. The pseudokinase MLKL mediates necroptosis via a molecular switch mechanism. *Immunity.* **39:** 443–453.

35. Degterev, A., J. L. Maki, and J. Yuan. 2013. Activity and specificity of necrostatin-1, small-molecule inhibitor of RIP1 kinase. *Cell Death Differ.* **20:** 366.

36. Kaiser, W. J., H. Sridharan, C. Huang, P. Mandal, J. W. Upton, P. J. Gough, C. A. Sehon, R. W. Marquis, J. Bertin, and E. S. Mocarski. 2013. Toll-like receptor 3-mediated necrosis via TRIF, RIP3, and MLKL. *J. Biol. Chem.* **288:** 31268–31279.

37. Sundaram, K., A. R. Mather, S. Marimuthu, P. P. Shah, A. J. Snider, L. M. Obeid, Y. A. Hannun, L. J. Beverly, and L. J. Siskind. 2016. Loss of neutral ceramidase protects cells from nutrient- and energy-deprivation-induced cell death. *Biochem. J.* **473:** 743–755.

38. Yang, W. S., and B. R. Stockwell. 2016. Ferroptosis: death by lipid peroxidation. *Trends Cell Biol.* **26:** 165–176.

39. Skouta, R., S. J. Dixon, J. Wang, D. E. Dunn, M. Orman, K. Shimada, P. A. Rosenberg, D. C. Lo, J. M. Weinberg, A. Linkermann, et al. 2014. Ferrostatins inhibit oxidative lipid damage and cell death in diverse disease models. *J. Am. Chem. Soc.* **136:** 4551–4556.

40. Zilka, O., R. Shah, B. Li, J. P. Friedmann Angeli, M. Griesser, M. Conrad, and D. A. Pratt. 2017. On the mechanism of cytoprotection by ferrostatin-1 and liproxstatin-1 and the role of lipid peroxidation in ferroptotic cell death. *ACS Cent. Sci.* **3:** 232–243.

41. Brennan-Minnella, A. M., A. S. J. Won, and R. A. Swanson. 2015. NADPH oxidase-2: linking glucose, acidosis, and excitotoxicity in stroke. *Antioxid. Redox Signal.* **22:** 161–174.

42. Dikalov, S. 2011. Cross talk between mitochondria and NADPH oxidases. *Free Radic. Biol. Med.* **51:** 1289–1301.

43. Sentelle, R. D., C. E. Senkal, W. Jiang, S. Ponnusamy, S. Gencer, S. P. Selvam, V. K. Ramshesh, Y. K. Peterson, J. J. Lemasters, Z. M. Szulc, et al. 2012. Ceramide targets autophagosomes to mitochondria and induces lethal mitophagy. *Nat. Chem. Biol.* **8:** 831–838.

44. Hannun, Y. A., and L. M. Obeid. 2008. Principles of bioactive lipid signalling: lessons from sphingolipids. *Nat. Rev. Mol. Cell Biol.* **9:** 139–150.

45. Kitatani, K., J. Idkowiak-Baldys, and Y. A. Hannun. 2008. The sphingolipid salvage pathway in ceramide metabolism and signaling. *Cell. Signal.* **20:** 1010–1018.

46. Clarke, C. J., B. X. Wu, and Y. A. Hannun. 2011. The neutral sphingomyelinase family: identifying biochemical connections. *Adv. Enzyme Regul.* **51:** 51–58.

47. Bai, A., C. Mao, R. W. Jenkins, Z. M. Szulc, A. Bielawska, and Y. A. Hannun. 2017. Anticancer actions of lysosomally targeted inhibitor, LCL521, of acid ceramidase. *PLoS One.* **12:** e0177805.

48. Kornhuber, J., P. Tripal, M. Reichel, C. Muhle, C. Rhein, M. Muehlbacher, T. W. Groemer, and E. Gulbins. 2010. Functional Inhibitors of Acid Sphingomyelinase (FIASMAs): a novel pharmacological group of drugs with broad clinical applications. *Cell. Physiol. Biochem.* **26:** 9–20.

49. Kölzer, M., N. Werth, and K. Sandhoff. 2004. Interactions of acid sphingomyelinase and lipid bilayers in the presence of the tricyclic antidepressant desipramine. *FEBS Lett.* **559:** 96–98.

50. Jenkins, R. W., J. Idkowiak-Baldys, F. Simbari, D. Canals, P. Roddy, C. D. Riner, C. J. Clarke, and Y. A. Hannun. 2011. A novel mechanism of lysosomal acid sphingomyelinase maturation: requirement for carboxyl-terminal proteolytic processing. *J. Biol. Chem.* **286:** 3777–3788.

51. Roth, A. G., D. Drescher, Y. Yang, S. Redmer, S. Uhlig, and C. Arenz. 2009. Potent and selective inhibition of acid sphingomyelinase by bisphosphonates. *Angew. Chem. Int. Ed. Engl.* **48:** 7560–7563.

52. Canals, D., D. M. Perry, R. W. Jenkins, and Y. A. Hannun. 2011. Drug targeting of sphingolipid metabolism: sphingomyelinases and ceramidases. *Br. J. Pharmacol.* **163:** 694–712.

53. Yang, W. S., R. SriRamaratnam, M. E. Welsch, K. Shimada, R. Skouta, V. S. Viswanathan, J. H. Cheah, P. A. Clemons, A. F. Shamji, C. B. Clish, et al. 2014. Regulation of ferroptotic cancer cell death by GPX4. *Cell.* **156:** 317–331.

54. Kushnareva, Y., A. N. Murphy, and A. Andreyev. 2002. Complex I-mediated reactive oxygen species generation: modulation by cytochrome c and NAD(P)+ oxidation-reduction state. *Biochem. J.* **368:** 545–553.

55. Nakagawa, T., S. Shimizu, T. Watanabe, O. Yamaguchi, K. Otsu, H. Yamagata, H. Inohara, T. Kubo, and Y. Tsujimoto. 2005. Cyclophilin D-dependent mitochondrial permeability transition regulates some necrotic but not apoptotic cell death. *Nature.* **434:** 652–658.

56. Bernardi, P., and F. Di Lisa. 2015. The mitochondrial permeability transition pore: molecular nature and role as a target in cardioprotection. *J. Mol. Cell. Cardiol.* **78:** 100–106.

57. Giorgio, V., E. Bisetto, M. E. Soriano, F. Dabbeni-Sala, E. Basso, V. Petronilli, M. A. Forte, P. Bernardi, and G. Lippe. 2009. Cyclophilin D modulates mitochondrial F0F1-ATP synthase by interacting with the lateral stalk of the complex. *J. Biol. Chem.* **284:** 33982–33988.

58. Schinzel, A. C., O. Takeuchi, Z. Huang, J. K. Fisher, Z. Zhou, J. Rubens, C. Hetz, N. N. Danial, M. A. Moskowitz, and S. J. Korsmeyer. 2005. Cyclophilin D is a component of mitochondrial permeability transition and mediates neuronal cell death after focal cerebral ischemia. *Proc. Natl. Acad. Sci. USA.* **102:** 12005–12010.

59. Hafner, A. V., J. Dai, A. P. Gomes, C. Y. Xiao, C. M. Palmeira, A. Rosenzweig, and D. A. Sinclair. 2010. Regulation of the mPTP by SIRT3-mediated deacetylation of CypD at lysine 166 suppresses age-related cardiac hypertrophy. *Aging (Albany NY).* **2:** 914–923.

60. Qiu, X., K. Brown, M. D. Hirschey, E. Verdin, and D. Chen. 2010. Calorie restriction reduces oxidative stress by SIRT3-mediated SOD2 activation. *Cell Metab.* **12:** 662–667.

61. Nieminen, A. L., A. K. Saylor, S. A. Tesfai, B. Herman, and J. J. Lemasters. 1995. Contribution of the mitochondrial permeability transition to lethal injury after exposure of hepatocytes to t-butylhydroperoxide. *Biochem. J.* **307:** 99–106.

62. Waldmeier, P. C., J. J. Feldtrauer, T. Qian, and J. J. Lemasters. 2002. Inhibition of the mitochondrial permeability transition by the non-immunosuppressive cyclosporin derivative NIM811. *Mol. Pharmacol.* **62:** 22–29.

63. Pap, E. H., G. P. Drummen, V. J. Winter, T. W. Kooij, P. Rijken, K. W. Wirtz, J. A. Op den Kamp, W. J. Hage, and J. A. Post. 1999. Ratio-fluorescence microscopy of lipid oxidation in living cells using C11-BODIPY(581/591). *FEBS Lett.* **453:** 278–282.

64. Novgorodov, S. A., T. I. Gudz, Y. E. Kushnareva, V. A. Roginsky, and Y. B. Kudrjashov. 1991. Mechanism accounting for the induction of nonspecific permeability of the inner mitochondrial membrane by hydroperoxides. *Biochim. Biophys. Acta.* **1058:** 242–248.

65. Spitzer, S., K. Volbracht, I. Lundgaard, and R. T. Karadottir. 2016. Glutamate signalling: A multifaceted modulator of oligodendrocyte lineage cells in health and disease. *Neuropharmacology.* **110:** 574–585.

66. Gao, M., P. Monian, Q. Pan, W. Zhang, J. Xiang, and X. Jiang. 2016. Ferroptosis is an autophagic cell death process. *Cell Res.* **26:** 1021–1032.

67. Ginsberg, M. D. 2008. Neuroprotection for ischemic stroke: past, present and future. *Neuropharmacology.* **55:** 363–389.

68. Kassmann, C. M., and K. A. Nave. 2008. Oligodendroglial impact on axonal function and survival - a hypothesis. *Curr. Opin. Neurol.* **21:** 235–241.

69. Li, X., E. Gulbins, and Y. Zhang. 2012. Oxidative stress triggers Ca-dependent lysosome trafficking and activation of acid sphingomyelinase. *Cell. Physiol. Biochem.* **30:** 815–826.

70. Gulbins, E., and P. L. Li. 2006. Physiological and pathophysiological aspects of ceramide. *Am. J. Physiol. Regul. Integr. Comp. Physiol.* **290:** R11–R26.

71. Zeidan, Y. H., and Y. A. Hannun. 2007. Activation of acid sphingomyelinase by protein kinase Cdelta-mediated phosphorylation. *J. Biol. Chem.* **282:** 11549–11561.

72. Zeidan, Y. H., B. X. Wu, R. W. Jenkins, L. M. Obeid, and Y. A. Hannun. 2008. A novel role for protein kinase Cdelta-mediated phosphorylation of acid sphingomyelinase in UV light-induced mitochondrial injury. *FASEB J.* **22:** 183–193.

73. Kim, Y. A., M. Y. Kim, and Y. S. Jung. 2013. Glutathione depletion by L-buthionine-S,R-sulfoximine induces apoptosis of cardiomyocytes through activation of PKC-delta. *Biomol. Ther. (Seoul).* **21:** 358–363.

74. Gorelenkova Miller, O., and J. J. Mieyal. 2015. Sulfhydryl-mediated redox signaling in inflammation: role in neurodegenerative diseases. *Arch. Toxicol.* **89:** 1439–1467.

75. Hill, B. G., and A. Bhatnagar. 2012. Protein S-glutathiolation: redox-sensitive regulation of protein function. *J. Mol. Cell. Cardiol.* **52:** 559–567.

76. Qiu, H., T. Edmunds, J. Baker-Malcolm, K. P. Karey, S. Estes, C. Schwarz, H. Hughes, and S. M. Van Patten. 2003. Activation of human acid sphingomyelinase through modification or deletion of C-terminal cysteine. *J. Biol. Chem.* **278:** 32744–32752.

77. Chatelut, M., M. Leruth, K. Harzer, A. Dagan, S. Marchesini, S. Gatt, R. Salvayre, P. Courtoy, and T. Levade. 1998. Natural ceramide is

unable to escape the lysosome, in contrast to a fluorescent analogue. *FEBS Lett.* **426:** 102–106.

78. Stancevic, B., and R. Kolesnick. 2010. Ceramide-rich platforms in transmembrane signaling. *FEBS Lett.* **584:** 1728–1740.

79. Tam, C., V. Idone, C. Devlin, M. C. Fernandes, A. Flannery, X. He, E. Schuchman, I. Tabas, and N. W. Andrews. 2010. Exocytosis of acid sphingomyelinase by wounded cells promotes endocytosis and plasma membrane repair. *J. Cell Biol.* **189:** 1027–1038.

80. Martinez, T. N., X. Chen, S. Bandyopadhyay, A. H. Merrill, and M. G. Tansey. 2012. Ceramide sphingolipid signaling mediates tumor necrosis factor (TNF)-dependent toxicity via caspase signaling in dopaminergic neurons. *Mol. Neurodegener.* **7:** 45.

81. Beckmann, N., D. Sharma, E. Gulbins, K. A. Becker, and B. Edelmann. 2014. Inhibition of acid sphingomyelinase by tricyclic antidepressants and analogons. *Front. Physiol.* **5:** 331.

82. Kincaid, B., and E. Bossy-Wetzel. 2013. Forever young: SIRT3 a shield against mitochondrial meltdown, aging, and neurodegeneration. *Front. Aging Neurosci.* **5:** 48.

83. Someya, S., W. Yu, W. C. Hallows, J. Xu, J. M. Vann, C. Leeuwenburgh, M. Tanokura, J. M. Denu, and T. A. Prolla. 2010. Sirt3 mediates reduction of oxidative damage and prevention of age-related hearing loss under caloric restriction. *Cell.* **143:** 802–812.

84. Finley, L. W., W. Haas, V. Desquiret-Dumas, D. C. Wallace, V. Procaccio, S. P. Gygi, and M. C. Haigis. 2011. Succinate dehydrogenase is a direct target of sirtuin 3 deacetylase activity. *PLoS One.* **6:** e23295.